

# A STATISTICAL MACHINE LEARNING APPROACH FOR ADAPTING REDUCED-ORDER MODELS USING PROJECTED GAUSSIAN PROCESS

XIAO LIU\* AND XINCHAO LIU†

**Abstract.** Projection-based model reduction is among the most widely adopted approaches for constructing parametric Reduced-Order Models (ROMs). Utilizing snapshot data from solving full-order governing equations, the Proper Orthogonal Decomposition (POD) computes the optimal basis modes that span a low-dimensional subspace where the ROM resides. Because a governing equation is often parameterized by a set of parameters, challenges immediately arise when one would like to investigate how systems behave differently over the parameter space (in design, diagnosis, control, uncertainty quantification and real-time operations). In this case, the optimal basis needs to be efficiently updated so as to adapt ROM that can accurately capture the variation of a system’s behavior over its parameter space. In this paper, we propose a Projected Gaussian Process (pGP) model and formulate the problem of adapting POD basis as a supervised statistical learning problem, for which the goal is to learn a mapping (injective) from the parameter space to the Grassmann Manifold that contains the optimal vector subspaces. To establish such a relationship, a mapping is found between the Euclidean space and the horizontal space of an orthogonal matrix that spans a reference subspace in the Grassmann Manifold. Then, a second mapping from the horizontal space to the Grassmann Manifold is established through the Exponential/Logarithm maps between the manifold and its tangent space. Finally, given a new parameter, the conditional distribution of a vector can be found in the Euclidean space using the Gaussian Process (GP) regression, and such a distribution is then projected to the Grassmann Manifold that enables us to find the optimal subspace, i.e., POD basis, for the new parameter. Compared with existing interpolation method, the proposed statistical learning approach allows us to optimally estimate (or tune) model parameters given data (i.e., the prediction/interpolation becomes problem-specific), and quantify the uncertainty associated with the prediction. Numerical examples are presented to demonstrate the advantages of the proposed pGP for adapting POD basis against parameter changes.

**Key words.** Reduced-Order Models, Proper Orthogonal Decomposition, Gaussian Process, Projected Gaussian Process, Grassmann Manifold

## 1. Introduction.

**1.1. Background and Problem Statement.** Consider the diffusion of chemical species, aeroelasticity of aircraft wings, flow of vehicles and predator-prey interactions, dynamics of such complex systems is typically described by a set of Partial Differential Equations (PDEs). Very often, the dimensions of these problems are extremely high due to the spatial discretization of the mathematical models (e.g., Computational Fluid Dynamics models or Finite Element Analysis with very large numbers of degrees of freedom). The prohibitive computational cost prevents us from repeatedly running numerical solvers under different parameter settings; often needed for design, diagnosis, prediction, uncertainty quantification and control problems[24, 25, 29]. Hence, when there exist low-dimensional patterns embedded in high-dimensional systems[16], Reduced-Order Models (ROMs) become indispensable in capturing the dominate behaviors of complex systems. Compared with data-driven surrogate models or meta models[3], ROM often preserve important system physics, such as stability[26, 4], passivity[31, 9], polynomial nonlinearities[27], etc.

Projection-based model reduction is among the most widely adopted approaches for constructing ROMs[16, 27]. The central idea behind projection-based ROM is to

---

\*H. Milton Stewart School of Industrial and Systems Engineering, Georgia Tech, Atlanta, GA (xiao.liu@isye.gatech.edu).

†H. Milton Stewart School of Industrial and Systems Engineering, Georgia Tech, Atlanta, GA (xliu975@gatech.edu).

project a high-dimensional governing equation to an optimal low-dimensional vector space spanned by orthogonal bases. Although searching for such bases may seem to be nontrivial considering the computational speed, accuracy and complex boundary conditions, the Proper Orthogonal Decomposition (POD)—applied to curves in Hilbert spaces  $\mathcal{H}$  of infinite dimension—provides a computationally efficient method for approximating data generated from full-order systems in an  $\ell_2$  sense[6]. This can be efficiently done by performing the thin Singular Value Decomposition (SVD) of the snapshot data matrix[16].

However, a governing equation is often parameterized by a set of parameters, and challenges immediately arise when one would like to investigate how systems behave differently over the parameter space (of the governing equation). In this case, the optimal basis needs to be updated so that the ROM can accurately capture the variation of a system’s behavior over its parameter space. As pointed out by [10, 32], the robustness and accuracy of an ROM are related to the reference parameters from which POD modes are derived. The accuracy of ROM determines the performance of any downstream machine learning models built on the low-dimensional ROM.

To elaborate, consider a governing equation with parameters  $\boldsymbol{\theta} = (\theta_1, \theta_2, \dots, \theta_d) \in \mathbb{P} \subset \mathbb{R}^d$ , where  $\mathbb{P}$  is the parameter space. Given  $\boldsymbol{\theta}$ , the solution of the system,  $x(t, \mathbf{s}; \boldsymbol{\theta})$ , is a space-time field,

$$(1.1) \quad (t, \mathbf{s}) \in [0, T] \times \mathbb{S} \mapsto x(t, \mathbf{s}; \boldsymbol{\theta})$$

where  $\mathbb{S}$  is the spatial domain and  $T > 0$ . Let  $\mathbf{x}(t; \boldsymbol{\theta}) = (x(t, \mathbf{s}_1; \boldsymbol{\theta}), x(t, \mathbf{s}_2; \boldsymbol{\theta}), \dots, x(t, \mathbf{s}_n; \boldsymbol{\theta}))$  be an  $n$ -dimensional vector representing the discretized solutions at a set of locations  $\{\mathbf{s}_1, \mathbf{s}_2, \dots, \mathbf{s}_n\} \in \mathbb{R}^n$  (say, using the Finite Element method), one can obtain the so-called *snapshot* data matrix,  $\mathbf{D}(\boldsymbol{\theta}) = [\mathbf{x}(t_1; \boldsymbol{\theta}); \mathbf{x}(t_2; \boldsymbol{\theta}); \dots; \mathbf{x}(t_{n_T}; \boldsymbol{\theta})]$ , where  $n_T$  is the number of temporal points. The POD method finds the optimal  $r$ -dimensional ( $r \ll n$ ) vector subspace  $\mathbb{W} \subset \mathbb{R}^n$  and an orthogonal projection,  $\mathcal{W} : \mathbb{R}^n \rightarrow \mathbb{W}$  such that the following distance is minimized[12]

$$(1.2) \quad \min_{\mathcal{W}} \sum_{i=1}^{n_T} \|\mathbf{x}(t_i; \boldsymbol{\theta}) - \mathcal{W}(\mathbf{x}(t_i; \boldsymbol{\theta}))\|^2$$

where  $\|\cdot\| = \sqrt{\langle \cdot, \cdot \rangle}$  with  $\langle \cdot, \cdot \rangle$  being the inner product of the Hilbert space. In particular, if the subspace  $\mathbb{R}^r$  is spanned by a matrix basis  $\boldsymbol{\Phi} = (\boldsymbol{\phi}_1, \boldsymbol{\phi}_2, \dots, \boldsymbol{\phi}_r) \in \mathbb{R}^{n \times r}$  with orthogonal columns and  $\boldsymbol{\Phi}^T \boldsymbol{\Phi} = \mathbf{I}_r$ , then,  $\mathbf{x}(t; \boldsymbol{\theta}) \approx \boldsymbol{\Phi} \mathbf{x}_r(t; \boldsymbol{\theta})$  and  $\boldsymbol{\Phi}$  can be found by minimizing the  $\ell_2$  error,  $\min_{\boldsymbol{\Phi}} \|\mathbf{D}(\boldsymbol{\theta}) - \boldsymbol{\Phi} \boldsymbol{\Phi}^T \mathbf{D}(\boldsymbol{\theta})\|_F^2$ , where  $\|\cdot\|_F$  is the Frobenius norm of matrices in the vector space. Following the Eckart-Young theorem[11], the solution of the minimization problem above is obtained by the thin Singular Value Decomposition (SVD) of the snapshot matrix  $\mathbf{D}(\boldsymbol{\theta})$ , i.e., let  $\mathbf{D}(\boldsymbol{\theta}) = \mathbf{U} \boldsymbol{\Sigma} \mathbf{V}^T$ ,  $\boldsymbol{\Phi} = [\mathbf{u}_1, \mathbf{u}_2, \dots, \mathbf{u}_r]$  retains the leading  $r$  columns of  $\mathbf{U}$ .

Hence, we see both the advantages and limitations of the POD approach above. The optimal POD basis, which is obtained from the snapshot data generated at the parameter setting  $\boldsymbol{\theta}$ , is optimal *and only optimal* for parameter  $\boldsymbol{\theta}$ . As shown in Figure 1, if data are already available from numerically solving the full-order governing equation repeatedly at a set of pre-determined parameter settings, it is possible to obtain the optimal basis for each parameter setting using the existing approach. However, for any new parameter in the parameter space, new basis modes (which is optimal or near optimal for the new parameter) is needed so that one can adapt the ROM

according to parameter changes. The lack of robustness against parameter change limits the applicability of ROMs for design, diagnosis, control, uncertainty quantification and real-time operations (e.g., digital twins), where parameter changes are common[1, 24, 25, 29].

In this paper, we formulate the problem of adapting POD basis as a supervised statistical learning problem, for which the goal is to learn a mapping between the parameter  $\theta$  and POD basis  $\Phi$  that spans a low-dimensional vector subspace. This subspace regression problem can be stated as follows:

*Given  $\{\theta_i, \Phi_i\}_{i=1}^k$  for  $\theta_i \in \mathbb{P}$ , the problem is to learn a mapping  $\mathcal{T} : \mathbb{P} \rightarrow \mathcal{ST}(r, n)$  from the parameter space  $\mathbb{P} \subset \mathbb{R}^d$  to a compact Stiefel manifold of matrices with orthogonal columns, which enables the prediction of the POD basis matrix  $\Phi^*$  given a new parameter  $\theta^*$  without numerically solving the computationally expensive full-order governing equation at  $\theta^*$  (see Figure 1).*

We address this problem by proposing a supervised statistical learning approach, known as the Projected Gaussian Process (pGP) regression. As shown in Figure 1, when (training) data are available by numerically solving the full-order governing equation repeatedly at a (usually small) number of parameter settings  $\{\theta_i\}_{i=1}^k$ , it is possible to obtain the optimal basis  $\{\Phi_i\}_{i=1}^k$  at each parameter setting, separately, using the existing approach. Once the proposed pGP regression learns the mapping between parameters and POD bases, a new basis can be generated given the new parameters, thus adapting the ROM for parameter changes (see Sec.3).

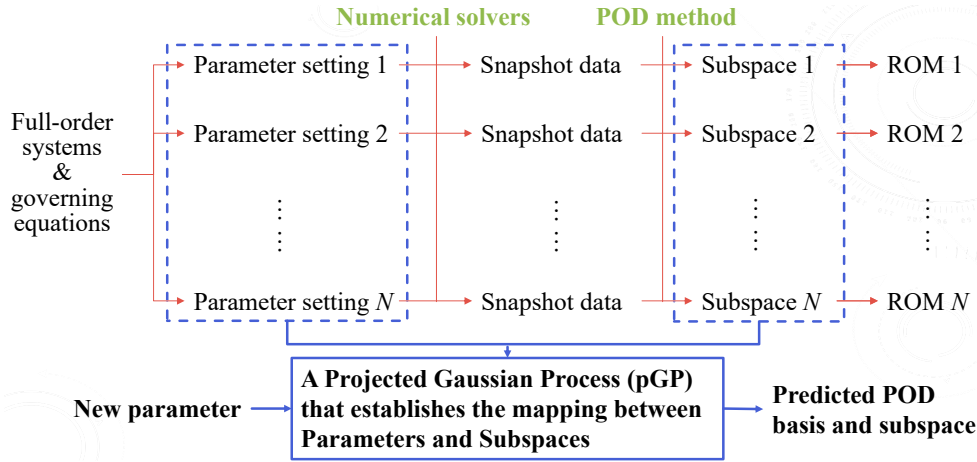


Fig. 1: A supervised statistical learning problem (based on the proposed Projected Gaussian Process) that establishes the mapping between parameters and POD basis modes so that ROMs can be adapted for parameter changes.

**1.2. Literature Review.** Various strategies have been proposed to adapt ROM for parameter changes. Figure 2 presents one possible way to group existing approaches into four categories. This figure is used to facilitate the explanations of different approaches as well as how the proposed approach is built upon prior work. The boundaries that separate different approaches may change if we examine these methods from different perspectives.

- Strategy I involves pre-computing a database, i.e., a library, of reduced-order bases[1, 15]. For applications where this approach is feasible, ROM can be updated

in real time over the set of parameters included in the database.

- Strategy II computes the first-order total derivatives of the POD modes with respect to a parameter[8], and a new POD basis, given a small change of the parameters from a base point, can be found through the first-order expansion in the parametric space.

- Strategy III involves different approaches that aim to interpolate or predict new POD bases from the observed parameter-POD basis pairs. In particular, the POD basis interpolation on Grassmann Manifolds have been extensively investigated[2, 30, 6, 23]. This approach is based on an important result that a subspace spanned by a POD basis is a point of the Grassmann Manifold that consists of  $r$ -dimensional subspaces in  $\mathbb{R}^n$ , where  $n$  and  $r$  are respectively the original and reduced-order dimensions. Hence, a tangent space, attached to a given base point in the Grassmann Manifold, can be constructed, and the subspaces from the Grassmann Manifold can be projected to the tangent space through a *logarithmic* map. After this critical step, interpolation can be done on the tangent space (such as the Lagrangian interpolation[2], inverse distance weighting[23], or Gaussian Process[13]), and the interpolated vector on the tangent space is eventually mapped back to the Grassmann Manifold through an *exponential* map. Hence, this method depends on the choice of the base point upon which the tangent space is attached to, and naturally requires the injective radius of the exponential map to be sufficiently large so that the approach is stable[12]. In contrast, the subspace angle interpolation approach directly computes the geometric distance between two subspaces by finding the principal angles between two POD bases[34]. The principal angles can be viewed as a series of angles required to rotate one subspace to form another, and such a distance metric is used to interpolate subspaces.

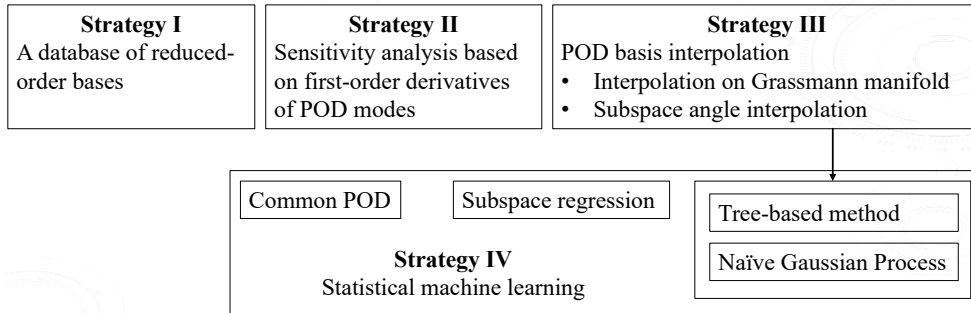


Fig. 2: Existing strategies to adapt ROM for parameter changes

- Strategy IV involves statistical machine learning to learn the mapping between parameters and POD bases (or the subspaces spanned by POD bases). Leveraging the key ideas from both the POD basis interpolation on Grassmann Manifold[2] and subspace angle interpolation[34], a regression tree-based approach on Grassmann Manifold was proposed in [18]. Following this approach, a tree is grown by repeatedly splitting the tree node (i.e., a binary partition the parameter space) to maximize the Riemannian distance between two subspaces (based on the principals angles) spanned by the predicted POD bases on the left and right daughter nodes. As a result, this tree-based approach effectively divides the parameter space into sub-regions, and find the optimal POD basis for each sub-region (which could generate useful insights on how a system’s behavior varies over the parameter space). This approach successfully combines the POD basis prediction problem into the classical framework of regression

trees, and appears to be more stable and conservative than the existing POD basis interpolation on Grassmann Manifolds (as the tree-based method only updates the POD basis when the parameter jumps from one sub-region to another in the parameter space). We also note that, this approach is useful for finding the POD basis when the dimension of the parameter space is high and the system behaviors have different sensitivity levels against different parameters. For those less important parameters, the tree-based approach effectively exclude those parameters from being used to split the tree (note that, the existing interpolation method does not automatically do this).

Other statistical learning approaches involve the use of Gaussian Process (GP). [13] directly used GP to capture the relationship between parameters and the matrices that determine the vectors on the tangent space of the Grassmann Manifold. Hence, given a new parameter setting, GP is used to predict a new vector in the tangent space, which yields the predicted subspace on the Grassmann Manifold through an exponential map. Note that, because GP performs prediction through a weighted linear combination of responses, this approach is similar to the existing Lagrangian POD basis interpolation on Grassmann Manifolds but essentially with different interpolation weights. For the reasons noted in Sec.3, we refer this approach as the native GP approach following the terminology in [21]. [20] proposed an approach known as Common POD (cPOD). In the context of engine injector design, a common POD basis is found for some base design geometry, the POD bases for other geometries are obtained by rescaling the common POD through a linear map. This approach requires sound domain knowledge of the system under consideration to determine the base design and establish the linear map between POD bases from the common POD. [35] proposed a GP subspace regression where the central idea is to directly construct a matrix-variate GP for the matrix bases such that the approach does not hinge on the differential geometric structures of the Gassmann manifold.

**1.3. Contributions of this Paper.** The prior work in the literature has shown the great potential of leveraging machine learning for adapting projection-based ROMs. The **main contribution** of this paper is to propose a new supervised statistical learning method, known as the Projected Gaussian Process (pGP) regression, that enables the learning of the mapping between parameters and POD bases. To our best knowledge, this method is *not yet available in the literature*. Computer code is also available as Supplementary Materials.

As a statistical machine learning approach, the proposed pGP provides some critical capabilities much needed for adapting ROMs against parameter changes:

*i*). Unlike existing interpolation method (e.g., Lagrangian interpolation), the statistical learning approach allows us to optimally estimate (or tune) model parameters based on the training data (i.e., the prediction becomes problem-specific). In contrast, when the Lagrangian interpolation is used, the Lagrange bases are computed from pre-existing equations which are independent of the problem or data of interest. Because the pGP model is always trained and optimized given the training dataset, such a flexibility potentially provides the opportunity to further improve the accuracy of ROM for the specific problem at hand (as shown in the numerical examples)

*ii*). The proposed pGP, as a statistical learning approach, provides the capability of parameter selection when constructing the mapping between parameters and POD bases. This capability is largely missing in the literature but is particularly important for systems with high-dimensional parameter space, i.e., not all parameters are equally important in terms of how they change the POD basis modes. If relevant parameters can be identified, one only needs to explore a reduced parameter space, with a lower

dimension, when investigating how system dynamics varies in the parameter space.

*iii*). Due to the parameter estimation/selection capabilities, the pGP approach naturally involves the use of global POD basis as its special case. When no parameter is identified as significant, the predicted POD basis matrices for different parameters, under the proposed pGP framework, become *i.i.d.* samples from a matrix-variate Gaussian distribution with the global POD basis matrix being the mean of this distribution (as shown in numerical Example II).

*iv*). The proposed pGP not only provides the point prediction of the POD basis, but also scientifically quantifies the uncertainty associated with the predicted POD basis as well as the output generated by ROMs. Such a capability of uncertainty quantification facilitates decision-making under uncertainty, and provides a critical link (as a future research path) from the proposed approach to a large body of literature on statistical experimental design and deep reinforcement learning for more efficient construction of ROMs by sequentially exploring the solution space of full-order models[14, 7].

The paper is organized as follows. In Section 2, we provide the preliminaries on POD basis interpolation. The proposed pGP approach is presented in Section 3. Comprehensive numerical examples and discussions are presented in Section 4. Section 5 concludes the paper.

**2. Preliminaries on POD basis interpolation.** This section provides preliminaries on the interpolation problem of POD basis modes. As discussed in Section 1.1, due to the computational cost associated with solving full-order governing equations, it is only possible to obtain the snapshot matrices for a relatively small number of parameters,  $\Lambda = \{\boldsymbol{\theta}_1, \boldsymbol{\theta}_2, \dots, \boldsymbol{\theta}_k\}$ , and obtain the optimal POD basis  $\Phi_1, \Phi_2, \dots, \Phi_k$  for each parameter in  $\Lambda$ . Hence, for any new parameter  $\boldsymbol{\theta}^* \notin \Lambda$ , the interpolation of POD basis is needed to obtain  $\Phi^*$ .

**Grassmann Manifold.** In honour of Hermann Grassmann, a Grassmann Manifold,  $\mathcal{G}(r, n) := \{\mathbb{W} \subset \mathbb{R}^n, \dim(\mathbb{W}) = r\}$ , is a differentiable manifold that collects all  $r$ -dimensional linear subspaces in  $\mathbb{R}^n$ [5]. Hence, the subspace  $\mathbb{W}$  is a point in  $\mathcal{G}(r, n)$  and the optimization problem in (1.2) essentially seeks the optimal point in  $\mathcal{G}(r, n)$  that minimizes the distance  $\sum_{i=1}^{n_T} \|\mathbf{x}(t_i; \boldsymbol{\theta}) - \mathcal{W}(\mathbf{x}(t_i; \boldsymbol{\theta}))\|^2$ .

**Stiefel manifold and a submersion.** A subspace in  $\mathcal{G}(r, n)$  is spanned by an orthogonal basis  $\Phi \in \mathbb{R}^{n \times r}$  ( $\Phi^T \Phi = \mathbf{I}_r$ ). A collection of  $n \times r$  matrices with orthogonal columns forms a compact Stiefel manifold denoted by  $\mathcal{ST}(r, n)$ [12]. Note that, if  $\Phi$  spans a subspace  $p \in \mathcal{G}(r, n)$ , so does  $\Phi \mathbf{J}$  for any  $r \times r$  matrix  $\mathbf{J}$  such that  $\mathbf{J}^T \mathbf{J} = \mathbf{I}_r$ . Therefore, there exists a fiber bundle

$$(2.1) \quad \pi : \Phi \in \mathcal{ST}(r, n) \mapsto \pi(\Phi) = p \in \mathcal{G}(r, n)$$

which indicates that any point  $p \in \mathcal{G}(r, n)$  can be represented by a point of  $\pi^{-1}(p)$ .

**Riemannian metric.** To establish the Riemannian metric on  $\mathcal{G}(r, n)$ , a unique tangent space  $\mathcal{T}_p \mathcal{G}(r, n)$  is attached to a point  $p \in \mathcal{G}(r, n)$ . The tangent space  $\mathcal{T}_p \mathcal{G}(r, n)$  has the same dimension of  $\mathcal{G}(r, n)$  (but is isomorphic to  $\mathbb{R}^{r \times (n-r)}$ , i.e.,  $\mathcal{T}_p \mathcal{G}(r, n) \simeq \mathbb{R}^{r \times (n-r)}$ ) and is equipped with a scalar product. For any two velocity vectors,  $v_1, v_2 \in \mathcal{T}_p \mathcal{G}(r, n)$ , we have

$$(2.2) \quad \langle v_1, v_2 \rangle := \langle \mathbf{Z}_1, \mathbf{Z}_2 \rangle = \text{trace}(\mathbf{Z}_1^T \mathbf{Z}_2)$$

where  $\mathbf{Z}_1$  and  $\mathbf{Z}_2$  are  $n \times r$  matrices from the horizontal space of  $\Phi = \pi^{-1}(p)$  denoted by  $\mathbb{H}_\Phi := \{\mathbf{Z} \in \mathbb{R}^{n \times r}; \mathbf{Z}^T \Phi = 0\}$ . In other words, given a base point  $p$ , the Grass-

mann Manifold inherits the Riemannian structure of the Stiefel manifold due to (2.1) and becomes a Riemannian manifold.

**Exponential and Logarithm maps.** For any point  $p \in \mathcal{G}(r, n)$  and the attached tangent space  $\mathcal{T}_p\mathcal{G}(r, n)$ , the Exponential map is defined as

$$(2.3) \quad \text{Exp}_p : v \in \mathcal{T}_p\mathcal{G}(r, n) \mapsto \pi(\Phi \mathbf{V}_Z \cos(\Sigma_Z) + \mathbf{U}_Z \sin(\Sigma_Z)) \in \mathcal{G}(r, n)$$

where  $\Phi = \pi^{-1}(p)$  and  $\mathbf{Z} = \mathbf{U}_Z \Sigma_Z \mathbf{V}_Z$  is the SVD of  $\mathbf{Z}$ .

For any point  $p \in \mathcal{G}(r, n)$  and a open set  $U_p := \{p' \in \mathcal{G}(r, n); \pi(\Phi) = p, \pi(\Phi') = p', \pi(\Phi)^T \pi(\Phi') \text{ is invertible}\}$ , the Logarithm map is defined as

$$(2.4) \quad \text{Log}_p : p' \in U_p \mapsto \text{Log}_p(p') \in \mathcal{T}_p\mathcal{G}(r, n).$$

**Existing POD interpolation method.** Within  $U_p$ , the Logarithm map  $\text{Log}_p$  is a diffeomorphism, and the one-one correspondence between  $v \in \mathcal{T}_p\mathcal{G}$  and  $p' \in U_p$  can be defined through the Exponential and Logarithm maps[12]. Hence, [2] described a well-known Lagrangian interpolation method for POD basis. In a nutshell, given the training data  $\{\theta_i, \Phi_i\}_{i=1}^k$ , subspaces corresponding to  $\theta_i$  are mapped to vectors  $v_i$  in the tangent space through the Logarithm map. Then, the interpolation of vectors can be done in the tangent space, and the interpolated vector  $v^*$  is mapped back to the Grassmann Manifold through the Exponential map. Such a POD basis interpolation algorithm is provided in Algorithm 2.1.

---

**Algorithm 2.1** POD basis interpolation on Grassmann Manifold

---

Input: Integers  $r$  and  $n$  ( $2r \leq n$ ),  $\{\theta_i, \Phi_i\}_{i=1}^k$ , and a target parameter  $\theta^*$ .

- Choose a matrix  $\Phi_0 \in \{\Phi_1, \Phi_2, \dots, \Phi_k\}$  such that  $\Phi_0^T \Phi_i$  is non-singular for all  $i$ .
- For each  $i = 1, 2, \dots, k$ , perform the thin SVD on  $\Phi_i(\Phi_0^T \Phi_i)^{-1} - \Phi_0 = \mathbf{U}_i \Sigma_i \mathbf{V}_i^T$ , and obtain a matrix  $\mathbf{Z}_i$

$$(2.5) \quad \mathbf{Z}_i = \mathbf{U}_i \arctan(\Sigma_i) \mathbf{V}_i^T.$$

- Compute an interpolated matrix and a thin SVD

$$(2.6) \quad \mathbf{Z}^* = \sum_{i=1}^k \prod_{i \neq j} \frac{\theta^* - \theta_j}{\theta_i - \theta_j} \mathbf{Z}_i = \mathbf{U}^* \Sigma^* \mathbf{V}^*$$

- Return an instability message if the largest singular value of  $\mathbf{Z}^*$  is greater than  $\pi/2$ . Otherwise, compute a  $n \times r$  matrix

$$(2.7) \quad \Phi^* = \Phi_0 \mathbf{V}^* \cos \Sigma^* + \mathbf{U}^* \sin \Sigma^*$$

where  $\sin$  and  $\cos$  only act on the diagonal of  $\Sigma^*$ .

**return** The interpolated POD basis  $\Phi^*$  for parameter  $\theta^*$ .

---

**3. Projected Gaussian Process for Adapting ROMs.** In this section, we describe a supervised statistical learning method, based on the proposed pGP, for adapting ROMs against parameter changes.

**3.1. Projection from  $\mathbb{R}^{nr-r}$  to  $\mathcal{G}(r, n)$ .** We first show that there exists an injective mapping from the Euclidean space  $\mathbb{R}^{nr-r}$  to the Grassmann Manifold  $\mathcal{G}(r, n)$ . This result will later enable us to define a GP on  $\mathbb{R}^{nr-r}$  and map it to  $\mathcal{G}(r, n)$ .

From the preliminaries in Sec.2, there is an isomorphism between the horizontal space  $\mathbb{H}_{\Phi}$  and the tangent space  $\mathcal{T}_p\mathcal{G}(r, n)$ , i.e.,  $\pi_{\mathbb{H}} : \mathbb{H}_{\Phi} \rightarrow \mathcal{T}_p\mathcal{G}(r, n)$ . Hence, it is possible to find a unique  $\mathbf{Z} \in \mathbb{H}_{\Phi}$  such that  $\pi_{\mathbb{H}}(\mathbf{Z}) = v \in \mathcal{T}_p\mathcal{G}(r, n)$ , and the matrix  $\mathbf{Z}$  is called the *horizontal lift* of the vector  $v \in \mathcal{T}_p\mathcal{G}(r, n)$ . The existence of such an isomorphism may suggest that a matrix-variate GP can be employed to model the relationship between  $\boldsymbol{\theta}$  and the matrix  $\mathbf{Z}$ . However, *it is important to point out that this seemingly natural approach needs to be carefully carried out because the matrix  $\mathbf{Z}$  should be defined on the horizontal space  $\mathbb{H}_{\Phi}$  given a base point  $p$ , rather than the Euclidean space  $\mathbb{R}^{n \times r}$* . Precisely speaking, if  $\mathbf{Z}$  is modeled as a GP with respect to the parameter  $\boldsymbol{\theta}$  on  $\mathbb{R}^{n \times r}$ , then, the point prediction,  $\hat{\mathbf{Z}}^*$ , is given by a linear combination of  $\mathbf{Z}_1, \mathbf{Z}_2, \dots, \mathbf{Z}_k$  based on the well-known results of GP regression[28]. Since  $\mathbf{Z}_1, \mathbf{Z}_2, \dots, \mathbf{Z}_k$  are in the horizontal space  $\mathbb{H}_{\Phi}$ , the point prediction  $\hat{\mathbf{Z}}^*$  remains in the same space. However, the uncertainty quantification or predictive internal of  $\hat{\mathbf{Z}}^*$  (or, the predicted  $\hat{\Phi}^*$ ) is problematic because a sample  $\mathbf{Z}$  from a Gaussian distribution on  $\mathbb{R}^{n \times r}$  does not necessarily belong to  $\mathbb{H}_{\Phi}$ .

To remedy this issue, we first present the following results:

**PROPOSITION 3.1.** *Given a basepoint  $p \in \mathcal{G}(r, n)$  and  $\Phi = [\phi_1, \dots, \phi_r]$  such that  $\pi(\Phi) = p$ , let  $\mathbf{y}$  be a  $(nr - r) \times 1$  vector,  $\tilde{\Phi} = \text{diag}\{\phi_1^T, \phi_2^T, \dots, \phi_r^T\}$  be a  $r \times nr$  matrix with orthogonal rows, and  $\mathbf{F} = [\mathbf{F}_1 | \mathbf{F}_2 | \dots | \mathbf{F}_r]$  be a  $(nr - r) \times nr$  matrix where each block  $\mathbf{F}_i$ ,  $i = 1, 2, \dots, r$ , is a  $(nr - r) \times n$  matrix that satisfies the following conditions: (i) for any block  $i$  ( $i = 1, 2, \dots, r$ ), only row  $(i - 1) \times (n - 1) + 1$  to row  $i \times (n - 1)$  contain non-zero entries; (ii) all non-zero row vectors are unit vectors; and (iii) all non-zero row vectors are orthogonal to each other (note that conditions (i)-(iii) imply  $\tilde{\Phi}\mathbf{F}^T = \mathbf{0}$ ). Then,*

$$(3.1) \quad \mathbf{Z} = \text{Mat}_{n,r}(\mathbf{F}^T \mathbf{y})$$

is a  $n \times r$  matrix that belongs to the horizontal space  $\mathbb{H}_{\Phi}$ , i.e.,  $\mathbf{Z}^T \Phi = \mathbf{0}$ .

Proof. Note that  $\mathbf{Z}$  belongs to the horizontal space of  $\Phi$ , i.e.,

$$(3.2) \quad \tilde{\Phi} \text{vec}(\mathbf{Z}) = \mathbf{0}$$

where  $\text{vec}(\mathbf{Z})$  is the column-wise vectorization of  $\mathbf{Z}$ , and  $\tilde{\Phi} = \text{diag}\{\phi_1^T, \phi_2^T, \dots, \phi_r^T\}$  is a  $r \times nr$  block diagonal matrix with orthogonal rows. Then, by introducing a  $(nr - r) \times nr$  matrix  $\mathbf{F}$  with orthogonal rows such that  $\tilde{\Phi}\mathbf{F}^T = \mathbf{0}$ , we have

$$(3.3) \quad \begin{pmatrix} \tilde{\Phi} \\ \mathbf{F} \end{pmatrix} \text{vec}(\mathbf{Z}) = \begin{pmatrix} \mathbf{0} \\ \mathbf{y} \end{pmatrix}$$

where  $\mathbf{y}$  is a  $(nr - r)$ -dimensional column vector.

Because  $\mathbf{F}\text{vec}(\mathbf{Z}) = \mathbf{y}$  is an underdetermined system, we may find  $\text{vec}(\mathbf{Z})$  by  $\mathbf{F}^\dagger \mathbf{y}$  where  $\mathbf{F}^\dagger = \mathbf{F}^T (\mathbf{F}\mathbf{F}^T)^{-1}$ . From conditions (i)-(iii) above,  $\mathbf{F}\mathbf{F}^T$  is an identity matrix, and  $\mathbf{F}^\dagger \mathbf{F}^T$  as shown in Proposition 3.1.

Here, the choice of  $\mathbf{F}$  depends on  $\Phi$  (and the basepoint  $p$  in Proposition 3.1) as it must satisfy conditions (i)-(iii). Let  $\tilde{\Phi} = [\tilde{\Phi}_1, \tilde{\Phi}_2, \dots, \tilde{\Phi}_r]$ , and let  $\tilde{\mathbf{F}} = [\tilde{\mathbf{F}}_1, \tilde{\mathbf{F}}_2, \dots, \tilde{\mathbf{F}}_r]$  be a  $(nr - r) \times nr$  proposal matrix where each block  $\tilde{\mathbf{F}}_i$  has the structure as specified by condition (i) above. Then, applying the Gram-Schmidt (G-S) process can be applied to the row vectors of each block  $\begin{pmatrix} \tilde{\Phi}_i \\ \tilde{\mathbf{F}}_i \end{pmatrix}$  (for  $i = 1, 2, \dots, r$ ) and normalizing each non-zero rows after the G-S process, we obtain  $\begin{pmatrix} \tilde{\Phi}_i \\ \tilde{\mathbf{F}}_i \end{pmatrix}$  where



$\mathbf{F}_i$  satisfies conditions (i)-(iii). Note that, the G-S process starts from the  $i$ -th row because the leading  $(i-1)$  rows of  $\tilde{\Phi}_i$  are zeros.

Proposition 3.1 implies that, from a vector  $\mathbf{y} \in \mathbb{R}^{nr-r}$ , it is possible to compute a matrix  $\mathbf{Z} = \text{Mat}_{n,r}(\mathbf{F}^\dagger \mathbf{y})$  that comes from the horizontal space  $\mathbb{H}_\Phi$ . In fact, it is not hard to understand why the dimension of  $\mathbf{y}$  is  $nr-r$ . Although there are  $n \times r$  elements in the matrix  $\mathbf{Z}$ , the constraint  $\mathbf{Z}^T \Phi = \mathbf{0}$  (i.e.,  $\mathbf{Z}$  must come from the horizontal space of  $\Phi$ ) takes  $r$  degree of freedom away, leaving behind  $nr-r$  degrees of freedom. Hence, for any basepoint  $p \in \mathcal{G}(r, n)$  and the tangent space  $\mathcal{T}_p \mathcal{G}(r, n)$ , we can define the following mapping from  $\mathbb{R}^{nr-r}$  to  $\mathcal{G}(r, n)$ ,

$$(3.4) \quad \mathcal{P}_p : \mathbf{y} \in \mathbb{R}^{nr-r} \mapsto \pi(\Phi \mathbf{V}_Z \cos(\Sigma_Z) + \mathbf{U}_Z \sin(\Sigma_Z)) \in \mathcal{G}(r, n).$$

Here,  $\mathcal{P}_p := \tilde{\mathcal{P}}_p \circ \text{Exp}_p$  where  $\tilde{\mathcal{P}}_p$  maps an  $(nr-r)$ -dimensional vector to the tangent space  $\mathcal{T}_p \mathcal{G}(r, n)$ ,

$$(3.5) \quad \tilde{\mathcal{P}}_p : \mathbf{y} \in \mathbb{R}^{nr-r} \mapsto v \in \mathcal{T}_p \mathcal{G}(r, n)$$

and the Exponential map,  $\text{Exp}_p$ , is defined in (2.3).

**3.2. Injectivity of the map,  $\mathcal{P}_p$ .** Although  $\mathcal{P}_p$  in (3.4) defines a map from  $\mathbb{R}^{nr-r}$  to  $\mathcal{G}(r, n)$ , it is important to guarantee that such a map is injective (i.e., a subspace in  $\mathcal{G}(r, n)$  can be uniquely determined by a vector in  $\Omega_p$ ). Proposition 3.2 below gives the condition for which  $\mathcal{P}_p$  is injective.

PROPOSITION 3.2. *Given a basepoint  $p \in \mathcal{G}(r, n)$ , there exists an open set  $\Omega_p \subset \mathbb{R}^{nr-r}$*

$$(3.6) \quad \Omega_p := \left\{ \mathbf{y} \in \mathbb{R}^{nr-r}; \|\mathbf{y}\| < \frac{\pi}{2} \right\}$$

such that the mapping  $\mathcal{P}_p$  is injective.

Proof. Consider an open set  $D_p \subset \mathcal{T}_p \mathcal{G}(r, n)$

$$(3.7) \quad D_p := \{v \in \mathcal{T}_p \mathcal{G}(r, n); \|v\| < \pi/2\}$$

where  $\pi/2$  is the injective radius on the Grassmann Manifold[12]. Hence, we seek an open set  $\Omega_p \subset \mathbb{R}^{nr-r}$  such that  $\mathcal{A}_p$  maps a vector  $\mathbf{y} \in \Omega_p$  to the open disk  $D_p$  above. Because  $\mathbf{Z} = \text{Mat}_{n,r}(\mathbf{F}^\dagger \mathbf{y})$ , we have

$$(3.8) \quad \begin{aligned} \mathbf{Z}^T \mathbf{Z} &= \begin{bmatrix} \mathbf{y}^T \mathbf{F}_1 \\ \mathbf{y}^T \mathbf{F}_2 \\ \vdots \\ \mathbf{y}^T \mathbf{F}_r \end{bmatrix} \begin{bmatrix} \mathbf{F}_1^T \mathbf{y} & \mathbf{F}_2^T \mathbf{y} & \cdots & \mathbf{F}_r^T \mathbf{y} \end{bmatrix} \\ &= \begin{bmatrix} \sum_{i=1}^{n-1} y_{(i-1) \times r+1}^2 & & & \\ & \sum_{i=1}^{n-1} y_{(i-1) \times r+2}^2 & & \\ & & \ddots & \\ & & & \sum_{i=1}^{n-1} y_{(i-1) \times r+r}^2 \end{bmatrix} \end{aligned}$$

Because the Riemannian metric on  $\mathcal{G}(r, n)$  is defined by  $\langle v_1, v_2 \rangle_p = \text{trace}(\mathbf{Z}_1^T \mathbf{Z}_2)$  given the basepoint  $p$ , we have

$$(3.9) \quad \|v\| = \sqrt{\text{trace}(\mathbf{Z}^T \mathbf{Z})} = \left( \sum_{i=1}^{nr-r} y_i^2 \right)^{\frac{1}{2}} = \|\mathbf{y}\|$$

which needs to be smaller than  $\pi/2$ . Hence, we have an open set  $\Omega_p$ , defined in (3.6), such that  $\mathcal{P}_p$  is injective.

**3.3. Prediction based on the pGP regression.** Proposition 3.1 suggests an effective approach to establish the mapping between the parameter and POD basis. In a nutshell, as illustrated in Figure 3, a GP can be established to describe the mapping between the parameters space  $\mathbb{R}^d$  and  $\mathbb{R}^{nr-r}$ , and then, the GP is projected to the Grassmann Manifold. As a result, for any new parameter  $\theta^*$ , a vector  $\mathbf{y}^*$  can be found and mapped back to the Grassmann Manifold to determine the optimal subspace onto which the full-order system is projected (equivalently, the POD basis matrix  $\Phi^*$ ).

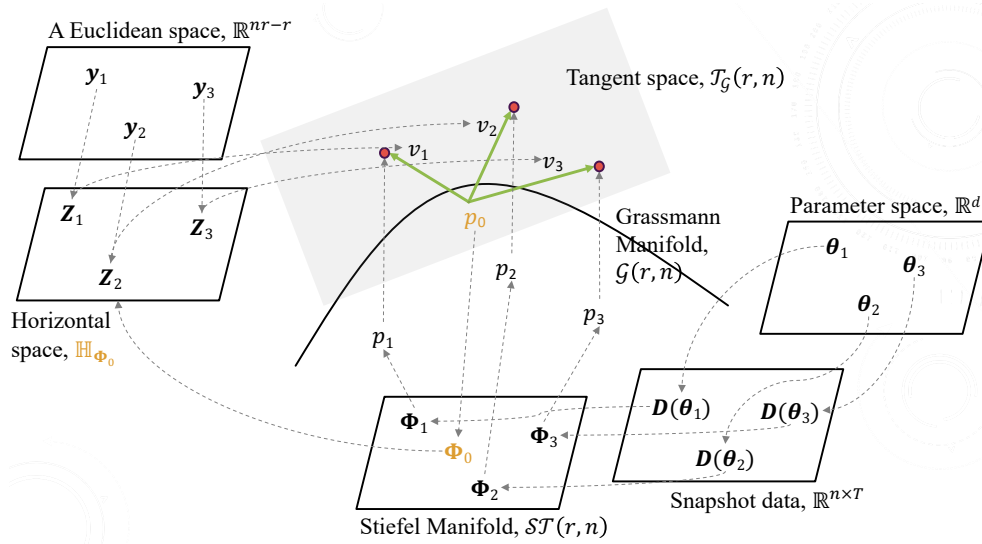


Fig. 3: A sketch of the key relationships between different spaces/manifolds involved in the pGP regression.

Let the vector  $\mathbf{y}$  follows the multivariate Gaussian distribution, i.e.,  $\mathbf{y} \sim \mathcal{N}(\mathbf{0}_{nr-r,1}, \mathbf{K})$  where  $\mathbf{K}$  is a  $(nr-r) \times (nr-r)$  symmetric and positive semi-definite matrix. Then,  $\mathbf{Z} = \text{Mat}_{n,r}(\mathbf{F}^\dagger \mathbf{y})$  follows a matrix-variate Gaussian,  $\mathbf{Z} \sim \mathcal{N}(\mathbf{0}_{n \times r}, \mathbf{F}^\dagger \mathbf{K} (\mathbf{F}^\dagger)^T)$  in the sense that  $\text{vec}(\mathbf{Z}) \sim \mathcal{N}(\mathbf{0}_{nr \times 1}, \mathbf{F}^\dagger \mathbf{K} (\mathbf{F}^\dagger)^T)$ . For a given point  $\mu \in \mathcal{G}(r, n)$  and a symmetric positive semi-definite matrix  $\mathbf{K} \in \mathbb{R}^{(nr-r) \times (nr-r)}$ , we say that a random point  $X \in \mathcal{G}(r, n)$  follows a Projected Gaussian Distribution (PGD) on  $\mathcal{G}(r, n)$

$$(3.10) \quad X \sim \mathcal{P}_\mu(\mathcal{N}(\mathbf{0}_{nr-r,1}, \mathbf{K}))$$

where the projection,  $\mathcal{P}_\mu : \mathbb{R}^{nr-r} \rightarrow \mathcal{G}(r, n)$ , is associated with the given point  $\mu$ . We denote the PGD by  $\mathcal{N}_{\mathcal{G}}(\mu, \mathbf{K})$ , and write  $X \sim \mathcal{N}_{\mathcal{G}}(\mu, \mathbf{K})$ ,  $\mu := \mu_{\mathcal{G}}(X) \in \mathcal{G}(r, n)$ , and  $\text{cov}_{\mathcal{G}}(X) := \mathbf{K}$ .

To obtain the mapping  $\mathcal{P}_\mu$  that connects  $\mathbb{R}^{nr-r}$  and  $\mathcal{G}(r, n)$  given a point  $\mu \in \mathcal{G}(r, n)$  and  $\Phi = \pi^{-1}(\mu) \in \mathcal{ST}(r, n)$ , we first introduce an operator  $\mathcal{P}_1$  such that  $\mathcal{P}_1(\mathbf{y}) = \text{Mat}_{n,r}(\mathbf{F}^\dagger \mathbf{y}) = \mathbf{Z}$ . Then, let  $\mathbf{Z} = \mathbf{U}_Z \Sigma_Z \mathbf{V}_Z^T$  be the thin SVD, an operator  $\mathcal{P}_2$  can be introduced that operates on the SVD of  $\mathbf{Z}$  such that  $\mathcal{P}_2(\mathbf{Z}) = \Phi \mathbf{V}_Z \cos(\Sigma_Z) + \mathbf{U}_Z \sin(\Sigma_Z)$  yields a  $n \times r$  matrix that spans a subspace in  $\mathcal{G}(r, n)$ . Hence, the mapping  $\mathcal{P}_\mu$  can be defined as

$$(3.11) \quad \mathcal{P}_\mu := \text{span} \circ \mathcal{P}_2 \circ \mathcal{P}_1$$

that maps a  $(nr - r) \times 1$  vector from  $\mathbb{R}^{nr-r}$  to a  $r$ -dimensional subspace in  $\mathcal{G}(r, n)$ .

**PROPOSITION 3.3.** *If  $X_i \sim \mathcal{N}_{\mathcal{G}_i}(\mu_i, \mathbf{K}_i)$  for  $i = 1, 2$ , then,  $(X_1, X_2)$  are jointly PGD on  $\mathcal{G}_1 \times \mathcal{G}_2$*

$$(3.12) \quad (X_1, X_2) \sim \mathcal{N}_{\mathcal{G}_1 \times \mathcal{G}_2} \left( \begin{pmatrix} \mu_1 \\ \mu_2 \end{pmatrix}, \tilde{\mathbf{K}} \right), \quad \tilde{\mathbf{K}} = \begin{pmatrix} \mathbf{K}_1, \mathbf{K}_{12} \\ \mathbf{K}_{12}^T, \mathbf{K}_2 \end{pmatrix}$$

Then, the conditional distribution of  $X_1$  given  $X_2 = p_2$  is given by

$$(3.13) \quad X_1 | (X_2 = p_2) \sim \mathcal{P}_{\mu_1}(\mathcal{MN}(\mathbf{u}_s, \mathbf{K}_s))$$

where  $\mathbf{u}_s = \mathbf{K}_{12}\mathbf{K}_2^{-1}\mathbf{s}$ ,  $\mathbf{K}_s = \mathbf{K}_1 - \mathbf{K}_{12}\mathbf{K}_2^{-1}\mathbf{K}_{12}^T$ ,  $\mathbf{s} = \mathcal{P}_{\mu_2}^{-1}(p_2)$ , and  $\mathcal{P}_{\mu_2}^{-1}$  is the inverse map.

Proposition 3.3 is obtained following a similar technique in [21]. Let  $\mathbb{A}_1 = \mathcal{P}_{\mu_1}^{-1}(p_1) = \{\mathbf{y} \in \mathbb{R}^{nr-r} : \mathcal{P}_{\mu_1}(\mathbf{Y}) = p_1\}$  be the preimage of  $p_1$  in  $\mathbb{R}^{nr-r}$  associated with  $\Phi_{\mu_1}$  given a point  $\mu_1$ , and let  $\mathbb{A}_2 = \mathcal{P}_{\mu_2}^{-1}(p_2)$  similarly be the preimage of  $p_2$ , then,

$$(3.14) \quad \begin{aligned} \Pr(X_1 | X_2 = p_2) &= \frac{\Pr(\mathbf{y}_1 \in \mathbb{A}_1, \mathbf{y}_2 \in \mathbb{A}_2)}{\Pr(\mathbf{y}_2 \in \mathbb{A}_2)} \\ &= \sum_{\mathbf{y}_1 \in \mathbb{A}_1, \mathbf{y}_2 \in \mathbb{A}_2} \frac{\mathcal{MN}(\mathbf{y}_2; \mathbf{0}, \mathbf{K}_2)}{\Pr(\mathbb{A}_2)} \frac{\mathcal{MN}((\mathbf{y}_1^T, \mathbf{y}_2^T)^T; \mathbf{0}, \tilde{\mathbf{K}})}{\mathcal{MN}(\mathbf{y}_2; \mathbf{0}, \mathbf{K}_2)} \\ &= \sum_{\mathbf{y}_1 \in \mathbb{A}_1, \mathbf{y}_2 \in \mathbb{A}_2} \lambda_{\mathbf{y}_2} \mathcal{MN}(\mathbf{y}_1; \mathbf{u}_{\mathbf{y}_2}, \mathbf{K}_{\mathbf{y}_2}) \end{aligned}$$

where  $\mathbf{u}_{\mathbf{y}_2} = \mathbf{K}_{12}\mathbf{K}_2^{-1}\mathbf{y}_2$ , and  $\mathbf{K}_{\mathbf{y}_2} = \mathbf{K}_1 - \mathbf{K}_{12}\mathbf{K}_2^{-1}\mathbf{K}_{12}^T$ .

Hence,

$$(3.15) \quad X_1 | (X_2 = p_2) \sim \mathcal{P}_{\mu_1}(\mathcal{MN}(\mathbf{u}_s, \mathbf{K}_s))$$

where  $\mathbf{s} = \mathcal{P}_{\mu_2}^{-1}(p_2)$ .

Once a PGD is obtained as described above, a Projected Gaussian Process (pGP) on Grassmann Manifold can be defined. We start with a multivariate GP defined in the Euclidean space. A collection  $\mathbf{y}$  of random vectors is a Multivariate GP (MGP) in  $\mathbb{R}^d$ , denoted by  $\mathbf{y} \sim \mathcal{MG}\mathcal{P}(f, \omega, \mathbf{K})$ , with a matrix-valued mean function  $f : \mathbb{R}^d \rightarrow \mathbb{R}^{nr-r}$ , kernel  $\omega : \mathbb{R}^d \times \mathbb{R}^d \rightarrow \mathbb{R}$  and  $\mathbf{K} \in \mathbb{R}^{(nr-r) \times (nr-r)}$ , if any finite collection of  $\mathbf{y}_1, \mathbf{y}_2, \dots, \mathbf{y}_k$  have a joint multivariate Gaussian distribution such that

$$(3.16) \quad [\mathbf{y}_1^T, \mathbf{y}_2^T, \dots, \mathbf{y}_k^T]^T \sim \mathcal{N}([f^T(\boldsymbol{\theta}_1), f^T(\boldsymbol{\theta}_2), \dots, f^T(\boldsymbol{\theta}_k)]^T, \boldsymbol{\Omega} \otimes \mathbf{K})$$

where  $\boldsymbol{\Omega} \in \mathbb{R}^{k \times k}$  with  $\Omega_{i,j} = \omega(\boldsymbol{\theta}_i, \boldsymbol{\theta}_j; \boldsymbol{\xi})$ . Then, a pGP on  $\mathcal{G}(r, n)$  can be defined as follows:

**Projected Gaussian Process.** A Projected Gaussian Process (pGP) on  $\mathcal{G}(r, n)$  is defined by

$$(3.17) \quad g \sim \mathcal{PG}\mathcal{P}(m, \omega, \mathbf{K})$$

where a collection  $(g(\boldsymbol{\theta}_1), g(\boldsymbol{\theta}_2), \dots, g(\boldsymbol{\theta}_k)) \sim \mathcal{P}_m(\mathcal{MG}\mathcal{P}(\mathbf{0}, \omega, \mathbf{K}))$  (i.e., a joint PGD),  $m(\boldsymbol{\theta}) := \mu_{\mathcal{G}}(g(\boldsymbol{\theta}))$  is the basepoint function and  $k(\boldsymbol{\theta}_i, \boldsymbol{\theta}_j) := \text{cov}_{\mathcal{G}}(g(\boldsymbol{\theta}_i), g(\boldsymbol{\theta}_j)) =$

$\omega(\theta_i, \theta_j)\mathbf{K}$  is the co-variance function in  $\mathbb{R}^{nr-r}$ . We denote the process by  $g \sim \mathcal{P}\mathcal{G}\mathcal{P}(m, \omega, \mathbf{K})$ .

Following Proposition 3.3, the joint distribution between the training output  $\mathbf{p}^{\text{train}} = (p_1, \dots, p_k)^T$  and test output  $p_*$  is given by:

$$(3.18) \quad \begin{pmatrix} p_* \\ \mathbf{p}^{\text{train}} \end{pmatrix} \sim \mathcal{N}_{\mathcal{G}_* \times \mathcal{G}_1 \times \dots \times \mathcal{G}_k} \left( \begin{pmatrix} m_* \\ \mathbf{m}^{\text{train}} \end{pmatrix}, \begin{pmatrix} \mathbf{K}_{**}, \mathbf{K}_* \\ \mathbf{K}_*^T, \mathbf{K}^{\text{train}} \end{pmatrix} \right)$$

where  $m_* = m(\theta_*)$ ,  $\mathbf{m}^{\text{train}} = (m(\theta_1), m(\theta_2), \dots, m(\theta_d))^T$ ,  $\mathbf{K}^{\text{train}} = \mathbf{\Omega} \otimes \mathbf{K} \in \mathbb{R}^{k(nr-r) \times k(nr-r)}$ ,  $\mathbf{K}_{**} = \omega(\theta_*, \theta_*)\mathbf{K} \in \mathbb{R}^{(nr-r) \times (nr-r)}$ ,  $\mathbf{K}_* = (\omega(\theta_*, \theta_1), \omega(\theta_*, \theta_2), \dots, \omega(\theta_*, \theta_d)) \otimes \mathbf{K} \in \mathbb{R}^{(nr-r) \times k(nr-r)}$ .

Finally,

$$(3.19) \quad p_* | \mathbf{p}^{\text{train}} \sim \mathcal{P}_{m_*}(\mathcal{M}\mathcal{N}(\mathbf{u}_*, \tilde{\mathbf{K}}_*))$$

where

$$(3.20) \quad \mathbf{u}_* = \mathbf{K}_*(\mathbf{K}^{\text{train}})^{-1}((\mathcal{P}_{m(\theta_1)}^{-1}(p_1))^T, (\mathcal{P}_{m(\theta_2)}^{-1}(p_2))^T, \dots, (\mathcal{P}_{m(\theta_d)}^{-1}(p_k))^T)^T$$

and

$$(3.21) \quad \tilde{\mathbf{K}}_* = \mathbf{K}_{**} - \mathbf{K}_*(\mathbf{K}^{\text{train}})^{-1}\mathbf{K}_*^T.$$

Hence, a point estimate of the subspace  $p_* \in \mathcal{G}(r, n)$  can be obtained by  $\hat{p}_* = \mathcal{P}_{m_*}(\mathbf{u}_*)$ . Because  $\mathbf{u}_*$  is the mean of the multivariate Gaussian distribution  $\mathcal{M}\mathcal{N}(\mathbf{u}_*, \tilde{\mathbf{K}}_*)$  defined in  $\mathcal{R}^{nr-r}$ ,  $\hat{p}_*$  is a maximum a posteriori probability (MAP) estimate. Also recall that  $\|\mathbf{u}_*\|$  needs to be smaller than  $\pi/2$  for  $\mathcal{P}_{m_*}$  to be injective. Hence, if  $\|\mathbf{u}_*\| > \pi/2$ , we shrink this vector  $\mathbf{u}_* \leftarrow \frac{\pi}{2} \frac{\mathbf{u}_*}{\|\mathbf{u}_*\|}$ , which is the projection of the original vector  $\mathbf{u}_*$  onto the surface of a  $(nr-r)$ -dimensional sphere. Similarly, the estimate  $\hat{\Phi}_*$  is obtained as  $\mathcal{P}_2 \circ \mathcal{P}_1(\mathbf{u}_*)$  such that  $\hat{p}_*$  is spanned by  $\hat{\Phi}_*$ .

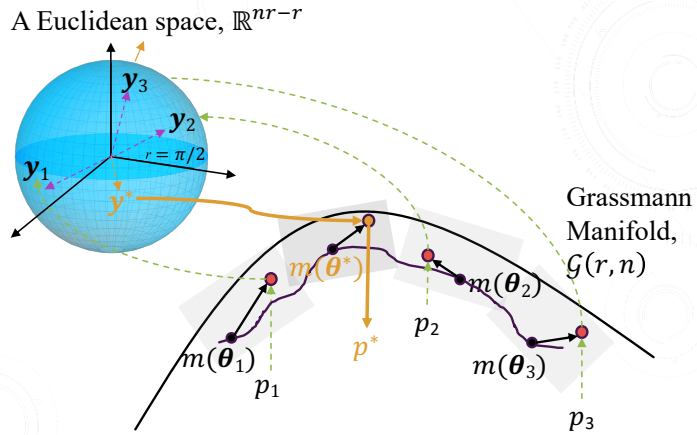


Fig. 4: An illustration of the subspace prediction using the pGP regression.

Figure 4 illustrate the process of predicting the optimal subspace using pGP. In this illustration, suppose that we obtain the snapshot data from three parameter settings  $\theta_1$ ,  $\theta_2$  and  $\theta_3$ , as well as the optimal subspaces  $p_1$ ,  $p_2$  and  $p_3$  that can be found using POD. The prediction of optimal subspace involves the following steps:

(i) Given the mean function  $m(\boldsymbol{\theta})$ , the three subspaces  $p_1$ ,  $p_2$  and  $p_3$  are firstly mapped to the Euclidean space  $\mathbb{R}^{nr-r}$  through the projection  $\mathcal{P}_{m(\boldsymbol{\theta})}^{-1}$ ; see (3.20). Note that,  $(\mathcal{P}_{m(\boldsymbol{\theta})}^{-1}(p))^T$  returns a  $(nr-r) \times 1$  column vector on  $\mathbb{R}^{nr-r}$ .

(ii) The three column vectors  $(\mathcal{P}_{m(\boldsymbol{\theta}_1)}^{-1}(p_1))^T$ ,  $(\mathcal{P}_{m(\boldsymbol{\theta}_2)}^{-1}(p_2))^T$  and  $(\mathcal{P}_{m(\boldsymbol{\theta}_3)}^{-1}(p_3))^T$  are used to predict a new column vector  $\mathbf{u}_*$ , for the new parameter  $\boldsymbol{\theta}_*$ , through a linear combination defined by a GP; see (3.20).

(iii) The covariance matrix  $\tilde{\mathbf{K}}_*$  is computed on  $\mathbb{R}^{nr-r}$ , which is exactly the same as the convectional GP. Steps (ii) and (iii) together yield a multivariate Gaussian distribution of  $\mathbf{y}_*$  on  $\mathbb{R}^{nr-r}$ , i.e.,  $\mathbf{y}_* \sim \mathcal{MN}(\mathbf{u}_*, \tilde{\mathbf{K}}_*)$ .

(iv) Finally, the Gaussian distribution of  $\mathbf{y}_*$  on  $\mathbb{R}^{nr-r}$  (or, the predicted column vector  $\mathbf{u}_*$  if only a point prediction is needed), is projected to the Grassmann Manifold through the projector  $\mathcal{P}_{m(\boldsymbol{\theta}_*)}$ .

#### 3.4. Discussions on model specification and parameter estimation.

A close examination of (3.19) reveals an important *difference* between how prediction is done by conventional GP and the proposed pGP. Using a conventional GP, the point predictor is a linear combination of the observations and the weights are determined by the covariance function (i.e., the point prediction does not depend the mean of the GP; a property well-known in the literature). For the proposed pGP, as indicated by (3.19), the point prediction does depend on the function  $m(\boldsymbol{\theta})$  that describes the relationship between the parameter and basepoint on the Grassmann Manifold. In other words, the choice of  $m(\boldsymbol{\theta})$  determines the mapping  $\mathcal{P}_m$ . Two approaches can be used to determine the function  $m(\boldsymbol{\theta})$ . The first approach is to fix the basepoint for all parameters, i.e.,  $m(\boldsymbol{\theta}) = \mu$ . which can be obtained using a global POD basis. The second approach is to use another regression model to determine  $m(\boldsymbol{\theta})$ , such as the tree-based method described in [18].

In addition, because  $n$  is usually large, a practical way to parameterize the  $(nr-r) \times (nr-r)$  covariance matrix  $\mathbf{K}$  is to let  $\mathbf{K} = \sigma_{\mathbf{K}}\mathbf{I}$  and estimate  $\sigma_{\mathbf{K}}$  from data. As for the kernel function  $\omega(\boldsymbol{\theta}_i, \boldsymbol{\theta}_j; \boldsymbol{\xi})$ , existing Gaussian, Exponential or other kernel functions can be used, and the parameter  $\boldsymbol{\xi}$  can be estimated from data. Hence, once  $m(\boldsymbol{\theta})$  is determined, the cross-validation-based approach can be used to estimate  $(\sigma_{\mathbf{K}}, \boldsymbol{\xi})$  by minimizing  $\sum_{i=1}^k \delta_i$ , where the cross validation error is given by  $\delta_i = \|\mathbf{D}(\boldsymbol{\theta}_i) - \hat{\boldsymbol{\Phi}}_{-i} \hat{\boldsymbol{\Phi}}_{-i}^T \mathbf{D}(\boldsymbol{\theta}_i)\|_F^2$ , and  $\hat{\boldsymbol{\Phi}}_{-i}$  is the estimated  $\boldsymbol{\Phi}_i$  excluding data  $\mathbf{D}(\boldsymbol{\theta}_i)$ .

Also note that, for systems with high-dimensional parameter space (i.e., relatively large  $d$ ), it is often the case that not all parameters are equally important in terms of how they affect the POD bases. In other words, the ROM can be sensitive to some parameters while independent of the others. Hence, when constructing the statistical learning model that establishes the mapping from parameter space to Grassmann Manifold, it is necessary to identify those relevant parameters. For the pGP model, one can achieve this goal using the Automatic Relevance Determination (ARD)[28]. To illustrate the idea, consider the squared Exponential kernel given by

$$(3.22) \quad \omega(\boldsymbol{\theta}_i, \boldsymbol{\theta}_j) = \xi_1^2 \delta_{\{\boldsymbol{\theta}_i = \boldsymbol{\theta}_j\}} + \xi_2^2 \exp \left\{ -\frac{(\boldsymbol{\theta}_i - \boldsymbol{\theta}_j)^T \mathbf{K}_\omega (\boldsymbol{\theta}_i - \boldsymbol{\theta}_j)}{2} \right\}$$

where  $\mathbf{K}_\omega = \text{diag}\{\xi_3^{-2}, \xi_4^{-2}, \dots, \xi_{d+2}^{-2}\}$ . Here, the parameters  $\xi_3, \xi_4, \dots, \xi_{d+2}$  play a role of characteristic length-scales for parameter  $\theta_1, \theta_2, \dots, \theta_d$ . If the estimated length-scales are very large, the corresponding parameters have little effects on the prediction and are practically removed from the model.

Finally, it is worth noting that the proposed pGP naturally involves the use of the

global POD basis as its special case. If  $\xi_1 = 0$  and the estimated  $\xi_3, \xi_4, \dots, \xi_{d+2}$  are all close to zero,  $\omega(\boldsymbol{\theta}_i, \boldsymbol{\theta}_j)$  becomes practically zero. In this case, (3.20) immediately implies that  $\mathbf{u}_* = \mathbf{0}$  and  $p_* | \mathbf{p}^{\text{train}} \sim \mathcal{P}_{m_*}(\mathcal{MN}(\mathbf{0}, \tilde{\mathbf{K}}_*))$ . If the global POD basis is chosen as the reference point (which spans a subspace in the Grassmann Manifold where the tangent space is attached to) and the basepoint function  $\mathbf{m}$  is invariant with  $\boldsymbol{\theta}$ , then, any subspace,  $p_i$ , corresponding to the ROM at parameter  $\boldsymbol{\theta}_i$  on the Grassmann Manifold can be seen as *i.i.d.* samples from a PGD,  $\mathcal{P}_{m_*}(\mathcal{MN}(\mathbf{0}, \tilde{\mathbf{K}}_*))$ . Hence, the point prediction,  $\hat{p}_*$ , is just the subspace spanned by the global POD basis.

**4. Numerical Examples.** Three numerical experiments are performed to demonstrate the proposed method: (i) flow around a circular cylinder; (ii) heat transfer in powder bed fusion additive manufacturing; and (iii) advection-diffusion processes.

**4.1. Example I: Flow around a Cylinder.** We first introduce the experiment setup and then present the experiment results.

**Experiment Setup.** In Example I, we consider the flow passing over a cylinder in a rectangle domain. The Lattice Boltzmann method is used to simulate the flow, i.e., to generate the training data for our model [22]. In particular, the Bhatnagar–Gross–Krook (BGK) approximation to the Navier-Stokes equation is:

$$(4.1) \quad \dot{f} + (\mathbf{v} \cdot \nabla)f = -\tau(f - \bar{f})$$

where  $f(\mathbf{x})$  be the phase-space density of fluids at location  $\mathbf{x}$ ,  $\mathbf{v}$  is the velocity,  $\tau$  is the timescale of which collisions happen, and  $\bar{f}$  represents the equilibrium state. In (4.1), the left side  $(\frac{\partial}{\partial t}f + (\mathbf{v} \cdot \nabla))f$  represents the streaming of particles, while the right side  $-\tau(f - \bar{f})$  represents the collision. The model assumes that the fluid locally relaxes to equilibrium over a characteristic timescale  $\tau$  related to the kinematic viscosity. The larger the  $\tau$  is, the larger is the kinematic viscosity.

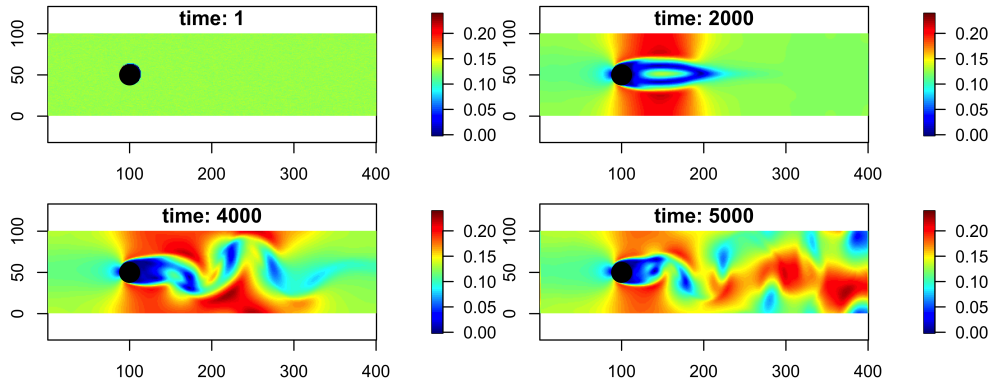


Fig. 5: Simulated flow velocity at times ( $\tau = 0.53$ )

The fluid equation (4.1) is solved by the Lattice Boltzmann method using the Python code in [22]. As shown in Figure 5, we consider a  $400 \times 100$  rectangle domain. A solid cylinder is placed at location  $(100, 50)$  with a radius of 13. The velocity goes from left to right with a magnitude of  $v = 2.3$  per time step, and 5000 time steps are simulated. The initial condition follows a Gaussian distribution with mean zero and standard deviation 0.01. Reflective boundary conditions are considered for the

cylinder, the top and the bottom boundaries, while the fluid is absorbed by the right boundary. Figure 5 shows the velocity of the flow, with  $\tau = 0.53$ , at times 1, 2000, 4000 and 5000. The Von Karman vortices are visible at times 4000 and 5000.

Figures 6 and 7 show the 1st, 4th, 7th and 10th POD modes for  $\tau = 0.53$  and  $\tau = 0.7$ , respectively. We see that the POD modes change as the parameter  $\tau$  changes, suggesting the necessity of adapting POD basis.

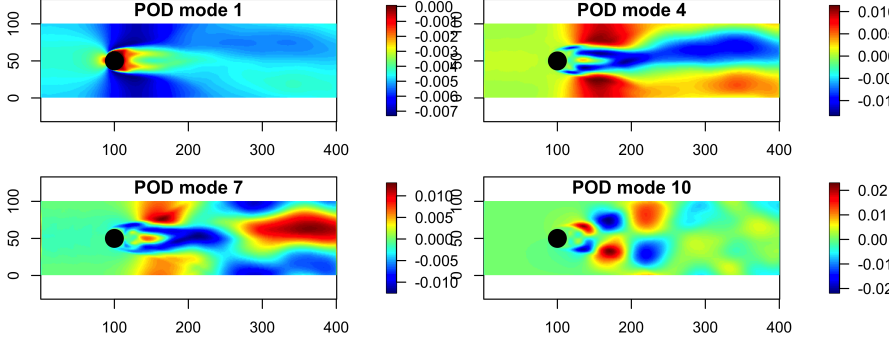


Fig. 6: The 1st, 4th, 7th and 10th POD modes for  $\tau = 0.53$

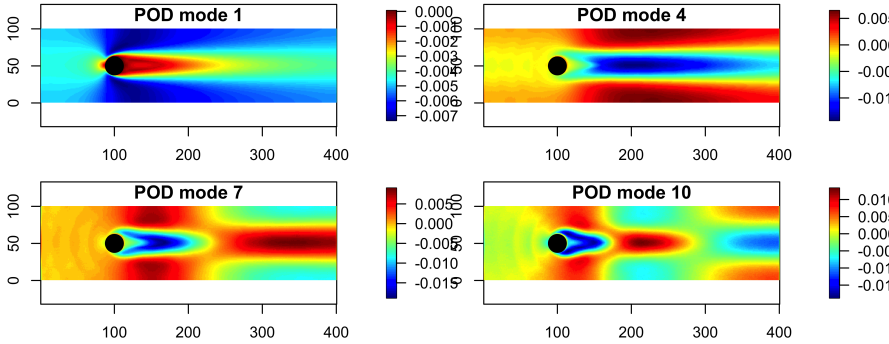


Fig. 7: The 1st, 4th, 7th and 10th POD modes for  $\tau = 0.7$

To evaluate the accuracy of the predicted ROM through cross validation, we generate data for 33 values of  $\tau$  ranging from 0.53 to 0.7 with a step size of 0.005. Then, the data are divided into a training and a testing sets. The training set includes the data generated from the following 11 parameter settings,

$$\tau^{\text{train}} = \{0.53, 0.545, 0.56, 0.575, 0.59, 0.605, 0.62, 0.635, 0.65, 0.665, 0.68\},$$

while the data generated from the remaining 22 parameter settings are used for testing.

In particular, we let  $m(\tau)$  yields a constant basepoint which is the subspace spanned by the global POD basis. The kernel  $\omega$  is chosen as  $\omega(\tau_i, \tau_j) = \xi_1 \exp(-\xi_2^{-1} |\tau_i - \tau_j|)$ , and  $\mathbf{K} = \sigma_{\mathbf{K}} \mathbf{I}$ . Note that,  $\mathbf{K}_* (\mathbf{K}^{\text{train}})^{-1}$  does not depend on  $\sigma_{\mathbf{K}}$  when  $\mathbf{K} = \sigma_{\mathbf{K}} \mathbf{I}$ , and only  $\xi_1$  and  $\xi_2$  are to be estimated by minimizing the cross-validation error. We obtain  $\xi_1 \approx 1$  and  $\xi_2 \approx 0.5$ .

**Experiment Results.** Figure 8 shows the out-of-sample testing errors for the proposed approach, the existing POD interpolation method, and the use of global POD bases. The errors are measured by the  $\ell_2$  Frobenius norm defined under (1.2). Some important observations are summarized as follows:

- The proposed approach yields much smaller  $\ell_2$  error than the existing POD interpolation method from testing cases #1 to #6, as well as from #19 to #22 (i.e., towards the two boundaries of the parameter space of  $\tau$ ). This consist observation suggests that the existing Lagrangian interpolation may have some stability issues for parameters near the boundaries of the parameter space, as investigated in [12]. In addition, as discussed in the introduction section, the proposed approach allows us to optimally estimate the model parameters based on data, while the coefficients of the Lagrangian interpolation are independent from data. Overall, the proposed approach yields smaller  $\ell_2$  error than the existing POD interpolation method for 21 out of the 22 testing cases (except for testing case #14 where the  $\ell_2$  errors are almost identical).

- The benefit of interpolating POD basis over the use of global POD bases is also demonstrated. The proposed approach yields smaller  $\ell_2$  errors than the use of the global POD bases for 17 out of the 22 testing cases.

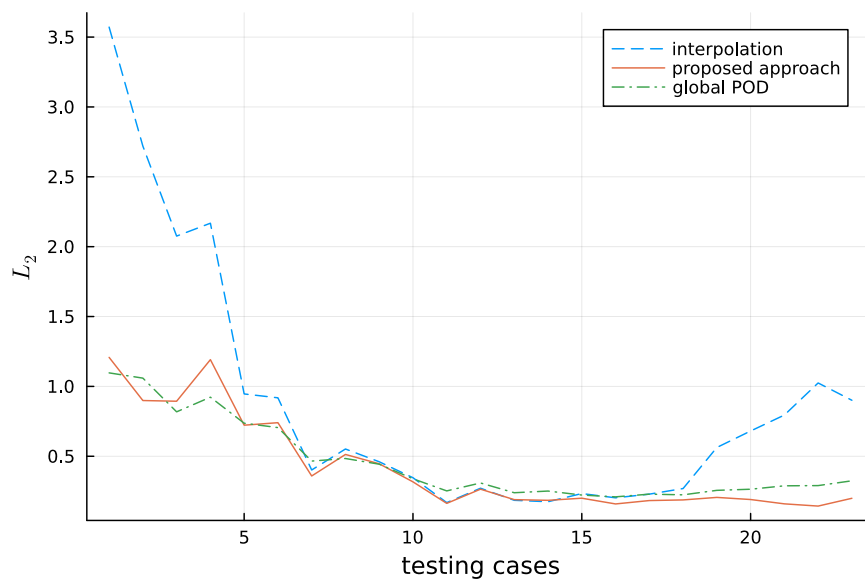


Fig. 8: Comparison of out-of-sample testing errors measured by the Frobenious norm

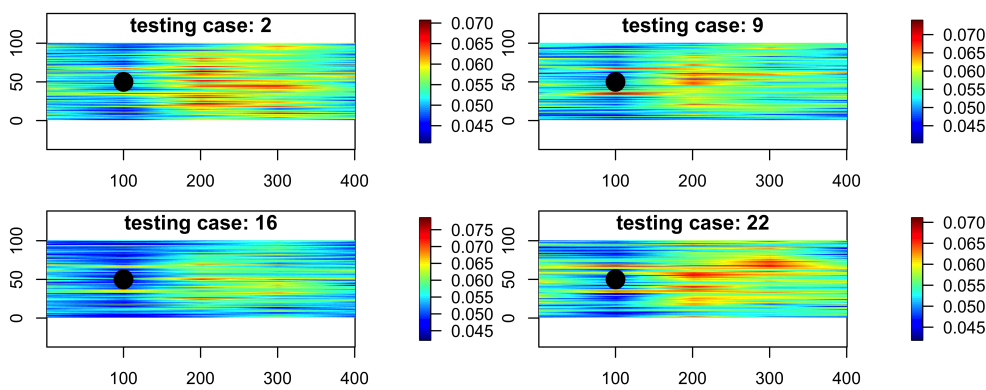


Fig. 9: Standard deviation associated with the ROM at time 100.



As a statistical learning approach, the proposed approach is capable of quantifying the uncertainty of the output generated from the ROM. Figure 9 shows the bootstrapping standard deviation of the output of the ROM for testing cases #1, #8, #15 and #22. Within each iteration, a subspace is randomly sampled from the distribution  $\mathcal{P}_{m_*}(\mathcal{MN}(\mathbf{u}_*, \tilde{\mathbf{K}}_*))$  obtained from (3.19), and an ROM is constructed on that sampled space. This procedure is repeated for 1000 times, and the standard deviation of the ROM output at time 100 is computed for each spatial location.

**4.2. Experiment II: Powder Bed Fusion Additive Manufacturing.** Powder Bed Fusion (PBF) with metals or polymers is one of the most common 3D printing technologies in industrial additive manufacturing (AM). PBF works by jointing powdered material point by point using energy sources such as lasers or electron beams. Thermal analysis is essential for product quality control which is key to spreading laser-based AM techniques [33] and manufacturing process design [17].

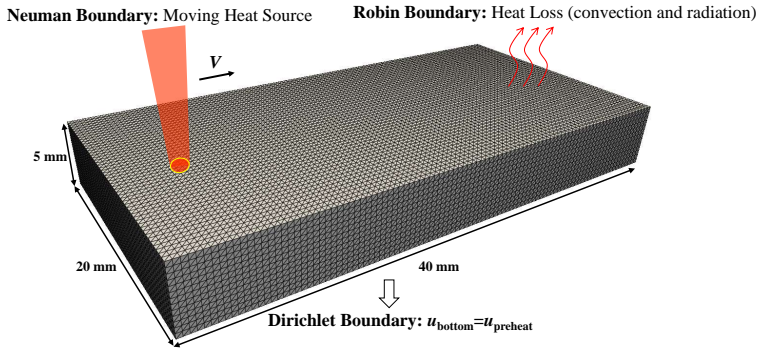


Fig. 10: Illustration of problem setup, spatial domain and boundary conditions.

**Experiment Setup.** In this example, we focus on the transient heat transfer in the single-track L-PBF (laser PBF) process as shown in Figure 10. The vacuum chamber is preheated to a specific temperature and the spatial domain is a combination of the solid substrate and the powder layer. The transient heat transfer process is governed by a PDE:

$$(4.2) \quad \rho c_p \frac{\partial u(x, t)}{\partial t} - \nabla \cdot k \nabla u(x, t) = 0, \quad (x, t) \in \Omega \times [0, t_f],$$

where  $\rho$  denotes the density,  $c_p$  is the specific heat capacity,  $k$  is the thermal conductivity of the material,  $u(x, t)$  represents the desired temperature over a space-time domain  $\Omega \times [0, t_f]$ . The heat flux boundary condition in PBF manufacturing processes is described as

$$(4.3) \quad (-k \nabla u(x, t)) \cdot \mathbf{n} = q_h + q_c + q_r, \quad (x, t) \in \partial\Omega \times [0, t_f],$$

where  $\mathbf{n}$  is the (outward) unit normal vector to the surface,  $q_h$ ,  $q_c$ , and  $q_r$  are the heat flux due to the heat source, convection and radiation, respectively.

A moving Gaussian heat source considered as follows:

$$(4.4) \quad q_h = -\frac{2\alpha\tau}{\pi\gamma^2} \exp\left(-\frac{2\|x - x^c(t)\|^2}{\gamma^2}\right), \quad x \in \partial\Omega_t,$$

where  $\partial\Omega_t$  denotes the top surface of domain,  $\alpha$  is the heat absorptivity,  $\tau$  is the laser power,  $\gamma$  is the effective laser (or electron) beam radius,  $x^c(t)$  is the center location of the energy beam at time  $t$ .

The convection and radiation, for  $x \in \partial\Omega_t \cup \partial\Omega_s$ , are modeled as

$$(4.5) \quad q_c(x, t) = h(u(x, t) - u_a), \quad q_r(x, t) = \sigma_s \epsilon (u(x, t)^4 - u_a^4),$$

where  $\partial\Omega_s$  denotes the side surfaces of domain,  $h$  is the heat convection coefficient,  $u_a$  is the ambient temperature,  $\sigma_s$  is the Stefan-Boltzmann constant,  $\epsilon$  is the emissivity of the material. The bottom surface of domain is defined with a Dirichlet boundary,  $u(x, \cdot) = u_b$ , where  $x \in \partial\Omega_b$ ,  $\partial\Omega_b$  denotes the bottom surface of domain and  $u_b$  is the fixed temperature. Finally, the initial condition is defined as  $u(\cdot, 0) = u_0$  where  $x \in \Omega$  and  $U_0$  is the initial temperature. Note that,  $\partial\Omega = \partial\Omega_t \cup \partial\Omega_s \cup \partial\Omega_b$ .

The Finite Element method (FEM) is used to solve the governing equations. Multiplying both sides of (4.2) by a test function  $\phi$  and integrating over  $\Omega$  gives

$$(4.6) \quad \int_{\Omega} \rho c_p \frac{\partial u(x, t)}{\partial t} \phi dV - \int_{\Omega} \nabla \cdot k \nabla u(x, t) \phi dV = 0, \quad (x, t) \in \Omega \times [0, t_f],$$

The solution  $u(x, t)$  and the test function are assumed to belong to Hilbert spaces. Unlike the original formulation that (4.2) holds for all points in  $\Omega$ , the weak formulation requires (4.6) to hold for all test functions in test function space. The Galerkin method assumes that the solution  $u(x, t)$  belongs to the same Hilbert space as the test functions. According to Green's first identity, (4.6) gives

$$(4.7) \quad \int_{\Omega} \rho c_p \frac{\partial u(x, t)}{\partial t} \phi dV + \int_{\Omega} k \nabla u(x, t) \cdot \nabla \phi dV + \int_{\partial\Omega} (-k \nabla u(x, t)) \cdot \mathbf{n} \phi dS = 0,$$

Then, the discretization by Galerkin method is applied to the weak formulation and the approximated solution  $u_d(x, t)$  is given by  $u_d(x, t) = \sum_{i=1}^N u_i(t) \psi_i(x)$ , where  $N$  is the number of nodes. For every test function  $\psi_j(x)$ , we have

$$(4.8) \quad \rho c_p \sum_{i=1}^N \frac{\partial u_i(t)}{\partial t} \int_{\Omega} \psi_i \psi_j dV + k \sum_{i=1}^N u_i(t) \int_{\Omega} \nabla \psi_i \nabla \psi_j dV + \sum_{i=1}^N \int_{\partial\Omega} (-k \nabla u_i(t) \psi_i) \cdot \mathbf{n} \psi_j dS = 0$$

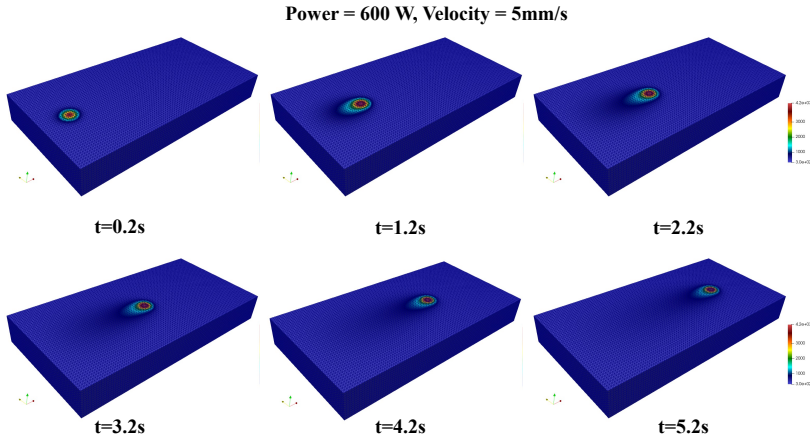


Fig. 11: Temperature field at 600W laser power with the heat source moving at a speed of 5mm/s.

We generate data for 7 laser power levels (in Watt):  $\{500, 550, 600, 650, 700, 750, 800\}$ , using the Finite Element method. As an illustration, Fig.11 shows the temperature

field at selected times. Since seven laser power levels are used to generate the data, a Leave-One-Out Cross-Validation (LOOCV) is performed to compare the model performance. Similar to Example 1, we let  $r = 10$  and  $m(\tau)$  be a constant basepoint which is the subspace spanned by the global POD basis. The kernel  $\omega$  is chosen as  $\omega(\tau_i, \tau_j) = \xi_1 \exp(-\xi_2^{-1}|\tau_i - \tau_j|)$ , and  $\mathbf{K} = \sigma_{\mathbf{K}}\mathbf{I}$ .

**Experiment Results.** Figure 12 shows LOOCV testing  $\ell_2$  errors for the proposed approach, the existing POD interpolation method, and the use of global POD bases. It is important note that,

- The use of global POD basis and the proposed pGP approach yield better and very similar results.

- More importantly, the proposed pGP is able to provide an explanation to such an observation. In short, this is because the proposed pGP (i) involves the use of global POD basis as its special case (due to its parameter selection capabilities), and (ii) successfully identifies that the ROM, in this example, is not sensitive to the change of parameters, and the use of the global POD basis becomes appropriate.

To elaborate, the kernel  $\omega$  is chosen as  $\omega(\tau_i, \tau_j) = \xi_1 \exp(-\xi_2^{-1}|\tau_i - \tau_j|)$  in this example. When LOOCV is performed, we note that the estimated values for  $\xi_2$  ranges between 40 to 80, effectively making  $\omega(\boldsymbol{\theta}_i, \boldsymbol{\theta}_j)$  close to zero. In this case, (3.19) immediately implies that  $\mathbf{u}_* = \mathbf{0}$  and  $p_*|\mathbf{p}^{\text{train}} \sim \mathcal{P}_{m_*}(\mathcal{MN}(\mathbf{0}, \tilde{\mathbf{K}}_*))$ . Because the global POD basis is chosen as the reference point, then, any subspace (corresponding different power levels  $\tau$ ) on the Grassmann Manifold can be seen as *i.i.d.* samples from a PGD,  $\mathcal{P}_{m_*}(\mathcal{MN}(\mathbf{0}, \tilde{\mathbf{K}}_*))$ . Hence, the point prediction,  $\hat{p}_*$ , is close to the subspace spanned by the global POD basis, justifying the observation in Figure 12.

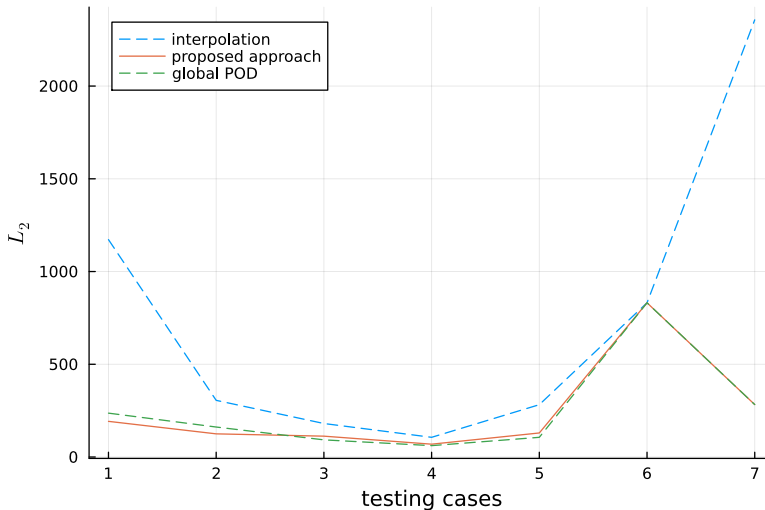


Fig. 12: Leave-One-Out Cross-Validation (LOOCV) errors.

**4.3. Experiment III: Advection-Diffusion Processes.** Advection-diffusion equations are widely used to describe the transfer of particles, energy, or other physical quantities inside a physical system due to diffusion and advection.

**Experiment Setup.** We consider a general form of advection-diffusion process  $\mathcal{A}(\boldsymbol{\theta})x(t, \mathbf{s}) = 0$ , where  $x(t, \mathbf{s})$  is a spatio-temporal process in space  $\mathbf{s} \in \mathbb{S} \subset \mathbb{R}^2$  and

time  $t \in [0, T]$ , and  $\mathcal{A}(\boldsymbol{\theta})$  is the advection-diffusion operator parameterized by  $\boldsymbol{\theta}$ :

$$(4.9) \quad \mathcal{A}x := \dot{x} + \vec{\boldsymbol{v}}^T \nabla x - \nabla \cdot [\boldsymbol{D} \nabla x]$$

where  $\vec{\boldsymbol{v}}$ ,  $\boldsymbol{D}$ ,  $\nabla$  and  $\nabla \cdot$  represent the velocity, diffusivity, decay, gradient and divergence, respectively. In this experiment,  $\mathbb{S}$  is a 2D rectangular domain.

Let  $\boldsymbol{x}(t; \boldsymbol{\theta}) = (x(t, \boldsymbol{s}_1; \boldsymbol{\theta}), \dots, x(t, \boldsymbol{s}_n; \boldsymbol{\theta}))$  be an  $n$ -dimensional vector representing the discretized solutions at a set of locations  $\{\boldsymbol{s}_1, \boldsymbol{s}_2, \dots, \boldsymbol{s}_n\} \in \mathbb{S}$ , we represent the advection-diffusion process by a dynamical system that is linear in state

$$(4.10) \quad \boldsymbol{x}(t; \boldsymbol{\theta}) = \boldsymbol{F} \boldsymbol{\alpha}(t; \boldsymbol{\theta}), \quad \dot{\boldsymbol{\alpha}}(t; \boldsymbol{\theta}) = \boldsymbol{G}(\boldsymbol{\theta}) \boldsymbol{\alpha}(t; \boldsymbol{\theta})$$

Here,  $\boldsymbol{F}$  is an  $n \times n$  matrix with its  $i$ -th row being  $\boldsymbol{f}(\boldsymbol{s}_i) = (f_1(\boldsymbol{s}_i), \dots, f_n(\boldsymbol{s}_i))$  where  $f_j(\boldsymbol{s}) = \exp(i \boldsymbol{k}_j^T \boldsymbol{s})$  is the Fourier basis function and  $\boldsymbol{k}_j$  is the spatial wavenumber,  $\boldsymbol{\alpha}(t) \in \mathbb{R}^n$  is the state vector,  $\boldsymbol{G}(\boldsymbol{\theta})$  is an  $n \times n$  state transition matrix operator, and the initial condition is denoted by  $\boldsymbol{x}_0$ . Note that, the matrix  $\boldsymbol{G}(\boldsymbol{\theta})$  depends on the parameters in (4.9) and is given by [19].

In projection-based ROM of parametric dynamic systems[6], we seek a ROM of the form to replace the original large-scale model (4.10) :

$$(4.11) \quad \boldsymbol{x}_r(t; \boldsymbol{\theta}) = \boldsymbol{F}_r \boldsymbol{\alpha}_r(t; \boldsymbol{\theta}), \quad \dot{\boldsymbol{\alpha}}_r(t; \boldsymbol{\theta}) = \boldsymbol{G}_r(\boldsymbol{\theta}) \boldsymbol{\alpha}_r(t; \boldsymbol{\theta})$$

where  $\boldsymbol{\alpha}_r(t)$  is the  $r$ -dimensional reduced-order state vector ( $r \ll n$ ),  $\boldsymbol{x}_r(t)$  is an approximation of  $\boldsymbol{\alpha}_r(t)$ , and  $\boldsymbol{F}_r \in \mathbb{R}^{n \times r}$  and  $\boldsymbol{G}_r \in \mathbb{R}^{r \times r}$ . Following the Galerkin's method, it is known that  $\boldsymbol{\alpha}_r(t) = \boldsymbol{\Phi}_\alpha^T \boldsymbol{\alpha}(t)$ ,  $\boldsymbol{G}_r = \boldsymbol{\Phi}_\alpha^T \boldsymbol{G} \boldsymbol{\Phi}_\alpha$  and  $\boldsymbol{F}_r = \boldsymbol{F} \boldsymbol{\Phi}_\alpha$ , where  $\boldsymbol{\Phi}_\alpha$  is a matrix basis with orthogonal columns. Given any parameter  $\boldsymbol{\theta}$ , we obtain from the snapshot data matrix  $\boldsymbol{D}(\boldsymbol{\theta}) = [\boldsymbol{x}(t_1; \boldsymbol{\theta}); \boldsymbol{x}(t_2; \boldsymbol{\theta}); \dots; \boldsymbol{x}(t_{n_T}; \boldsymbol{\theta})]$  the POD basis  $\boldsymbol{\Phi}$ . Because  $\boldsymbol{x}(t; \boldsymbol{\theta}) = \boldsymbol{F} \boldsymbol{\alpha}(t; \boldsymbol{\theta})$ , i.e.,  $\boldsymbol{x}(t; \boldsymbol{\theta})$  is the left unitary transformation of  $\boldsymbol{\alpha}(t; \boldsymbol{\theta})$ , the invariance property of SVD to unitary transformation yields  $\boldsymbol{\Phi}_\alpha = \boldsymbol{F} \boldsymbol{\Phi}$ [16].

To evaluate the accuracy of adapting ROM using the proposed pGP, we let  $\boldsymbol{v} = (v_x, 0.005)^T$ ,  $\boldsymbol{D} = \text{diag}\{0.001, 0.001\}$  and generate data by letting  $v_x$  vary from -0.02 to 0.02 with a step size of 0.001. The same initial condition is used for all  $v_x$  values. In total, a number of 42 snapshot data matrices are generated for 42 values of  $v_x$ . The data are divided into a training and a testing sets. The training set includes the data generated from the following 11 parameter settings,  $v_x^{\text{train}} = \{-0.016, -0.012, -0.008, -0.004, -0.002, 0, 0.004, 0.008, 0.012, 0.016, 0.02\}$ , while the data generated from the remaining 31 parameter settings are used for testing. In the testing phase, the trained pGP model is used to predict the optimal POD basis  $\boldsymbol{\Phi}_\alpha$  for a given value of  $v_x$ , and the corresponding ROM (4.11) is constructed. Then, we solve the ROM to obtain the reduced-order solution  $\boldsymbol{x}_r(t)$  and re-construct the full-order solutions by  $\boldsymbol{x}(t) = \boldsymbol{\Phi} \boldsymbol{x}_r(t)$ .

**Experiment Results.** To show and compare the performance of different approaches, Figure 13 shows the (re-constructed) solution from the proposed pGP, (re-constructed) solution from the existing POD interpolation approach, (re-constructed) solution using the global POD, and the (ground truth) solution by directly solving the full-order system. For illustrative purposes, these figures show the results for  $v_x = 0.006$  (which is not included in the training dataset) at times 1 (the initial condition), 5, 10, and 15. We see that the accuracy of the (reconstructed) solutions obtained from the existing POD interpolation approach deteriorates starting from time 5, while the proposed pGP approach provides more accurate solutions.

To further show the advantages of the proposed pGP approach, Figure 14 presents the comparison of the overall accuracy for all testing cases. The improvement by the proposed pGP is clearly observed.

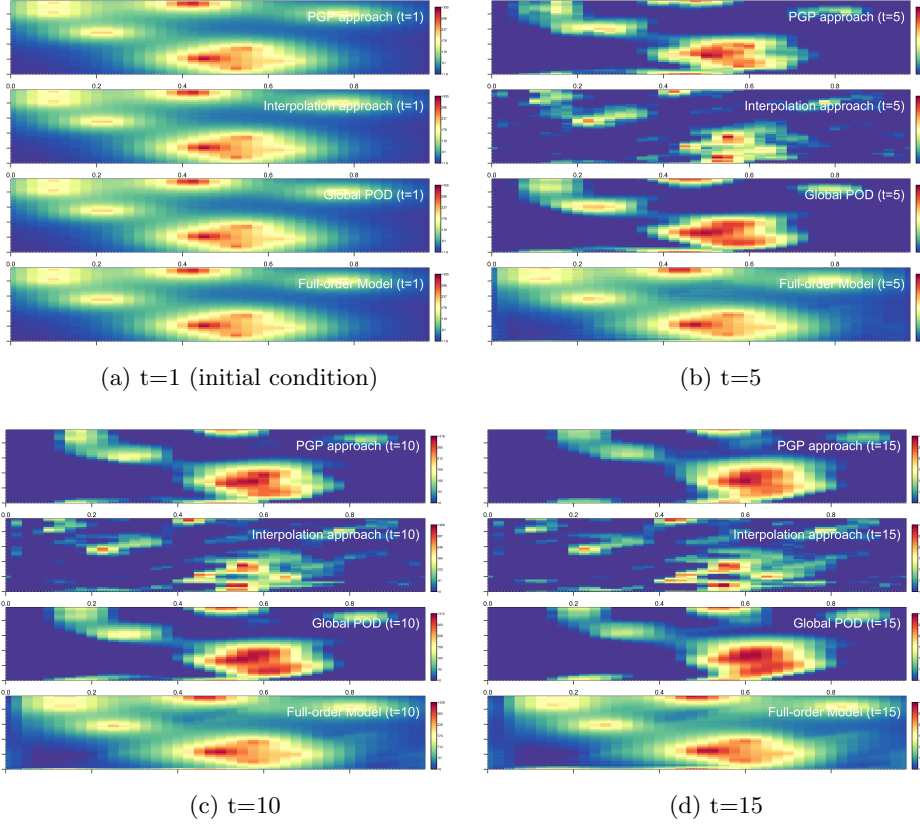


Fig. 13: Comparison between the proposed pGP (row 1 of each subfigure), the existing POD interpolation approach (row 2), the use of global POD (row 3), and the (ground truth) solution by directly solving the full-order system (row 4) at  $v_x = 0.006$

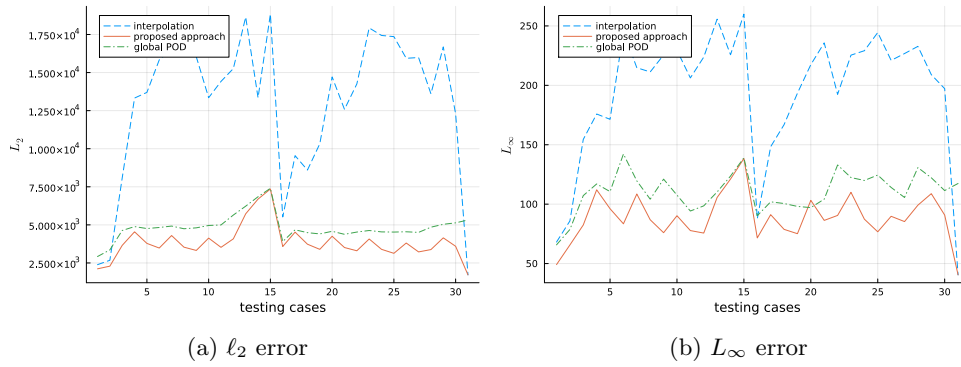


Fig. 14: Comparison between the proposed approach, existing POD interpolation approach and the use of global POD for constructing ROM against parameter changes.

**4.4. Code and Data.** Code and data are submitted as Supplementary Materials. Because the size of the dataset is about 3.5GB, users may download the data from the following link: [https://drive.google.com/file/d/1Ub\\_TnaB0--cW3tcNLSr2qiVdliH2xdJ/view?usp=sharing](https://drive.google.com/file/d/1Ub_TnaB0--cW3tcNLSr2qiVdliH2xdJ/view?usp=sharing).

**5. Conclusions.** This work successfully demonstrated the great potential of introducing machine learning to the field of robust reduced-order modeling. A supervised learning problem, based on the proposed pGP regression, has been developed to predict the optimal POD basis. The proposed approach leverages an injective mapping from the parameter space to the Grassmann Manifold that contains the optimal vector subspaces. The condition for such a mapping to be injective has been obtained, and sufficient technical details were presented for predicting POD basis using the proposed pGP regression. Numerical experiments showed that the proposed pGP approach not only improves the accuracy of ROMs against parameter change, but also enables uncertainty quantification and parameter selection, potentially reducing the dimension of the parametric space when adapting ROMs. We would also like to point out that there exists a critical link between the proposed pGP and statistical experimental design/reinforcement learning that enable sequential exploration of a system's behavior in a reduced parameter space. This link is expected to create important future research trajectories, potentially attracting more researchers into this field and making tangible contributions to Scientific Machine Learning research and its applications.

#### REFERENCES

- [1] D. AMSALLEM, J. CORTIAL, AND C. FARHAT, *On-demand cfd-based aeroelastic predictions using a database of reduced-order bases and models*, in 47th AIAA Aerospace Sciences Meeting Including the New Horizons Forum and Aerospace Exposition, Orlando, Florida, 2009, <https://doi.org/10.2514/6.2009-800>.
- [2] D. AMSALLEM AND C. FARHAT, *Interpolation method for adapting reduced-order models and application to aeroelasticity*, AIAA Journal, 7 (2008), pp. 1803–1813.
- [3] R. BARTON AND M. MECKESHEIMER, *Chapter 18 metamodel-based simulation optimization*, in Simulation, S. Henderson and B. Nelson, eds., Elsevier, 2006, pp. 535–574.
- [4] S. BATOOL, M. IMRAN, AND M. IMRAN, *Stability preserving model reduction technique for weighted and limited interval discrete-time systems with error bound*, IEEE Transactions on Circuits and Systems II: Express Briefs, 68 (2021), pp. 3281–3285, <https://doi.org/10.1109/TCSII.2021.3066890>.
- [5] T. BENDOKAT, R. ZIMMERMANN, AND P. A. ABSIL, *A grassmann manifold handbook: Basic geometry and computational aspects*, arXiv:2011.13699v, (2020).
- [6] P. BENNER, S. GUGERCIN, AND K. WILLCOX, *A survey of projection-based model reduction methods for parametric dynamical systems*, SIAM Review, 57 (2015), pp. 483–531.
- [7] T. BLAU, E. V. BONILLA, I. CHADES, AND A. DEZFOULI, *Optimizing sequential experimental design with deep reinforcement learning*, The 39th International Conference on Machine Learning, (2022).
- [8] A. H. J. BORRGAARD AND D. PELLETIER, *On the use of sensitivity analysis to improve reduced-order models*, in 4th Flow Control Conference, Seattle, Washington, 2008, <https://doi.org/10.2514/6.2008-4192>.
- [9] T. BREITEN AND B. UNGER, *Passivity preserving model reduction via spectral factorization*, Automatica, 142 (2022), p. 110368, <https://doi.org/10.1109/TCSII.2021.3066890>.
- [10] T. BUI-THANH, K. WILLCOX, AND O. GHATTAS, *Model reduction for large-scale systems with high-dimensional parametric input space*, SIAM Journal on Scientific Computing, 6 (2008), pp. 3270–3288.
- [11] C. ECKART AND G. YOUNG, *The approximation of one matrix by another of lower rank*, Psychometrika, 1 (1936), pp. 3170–3200.
- [12] O. FRIDERIKOS, E. BARANGER, M. OLIVE, AND D. NERON, *On the stability of pod basis interpolation on grassmann manifolds for parametric model order reduction*, Computational Mechanics, 70 (2020), pp. 181–204.

- [13] D. G. GIOVANIS AND M. D. SHIELDS, *Data-driven surrogates for high dimensional models using gaussian process regression on the grassmann manifold*, Computer Methods in Applied Mechanics and Engineering, 370 (2020), p. 113269.
- [14] D. R. IVANOVA, A. FOSTER, S. KLEINEGESSE, M. U. GUTMANN, AND T. RAINFORTH, *Implicit deep adative design: Policy-based experimental design without likelihoods*, NeurIPS 2021, (2021).
- [15] M. G. KAPTEYN, D. J. KNEZEVIC, D. B. P. HUYNH, M. TRAN, AND K. WILLCOX, *Data-driven physics-based digital twins via a library of component-based reduced-order models*, International Journal of Numerical Methods in Engineering, 13 (2020), pp. 2986–3003.
- [16] J. N. KUTZ, S. L. BRUNTON, B. W. BRUNTON, AND J. L. PROCTOR, *Dynamic mode decomposition: data-driven modeling of complex systems*, SIAM, 2016.
- [17] S. LIAO, T. XUE, J. JEONG, S. WEBSTER, K. EHMANN, AND J. CAO, *Hybrid full-field thermal characterization of additive manufacturing processes using physics-informed neural networks with data*, arXiv preprint arXiv:2206.07756, (2022).
- [18] X. LIU AND X. C. LIU, *Regression trees on grassmann manifold for adapting reduced-order models*, AIAA Journal, 61 (2023), pp. 1318–1333.
- [19] X. LIU, K. M. YEO, AND S. Y. LU, *Statistical modeling for spatio-temporal data from stochastic convection-diffusion processes*, Journal of the American Statistical Association, 117 (2022), pp. 1482–1499.
- [20] S. MAK, C. L. SUNG, X. WANG, S. T. YE, Y. H. CHANG, V. R. JOSEPH, V. YANG, AND C. F. J. WU, *An efficient surrogate model for emulation and physics extraction of largeeddy simulations*, Journal of the American Statistical Association, 113 (2018), pp. 1443–1456.
- [21] A. MALLASTO AND A. FERAGEN, *Wrapped gaussian process regression on riemannian manifolds*, in 2018 IEEE/CVF Conference on Computer Vision and Pattern Recognition, 2018, pp. 5580–5588, <https://doi.org/10.1109/CVPR.2018.00585>.
- [22] P. MOCZ, *Create your own lattice boltzmann simulation (with python)*, (2020), <https://github.com/pmocz/latticeboltzmann-python/blob/main/latticeboltzmann.py>.
- [23] R. MOSQUERA, A. HAMDOUNI, A. E. HAMIDI, AND C. ALLERY, *Pod basis interpolation via inverse distance weighting on grassmann manifolds*, Discrete and Continuous Dynamical Systems–Series S, 12 (2019), pp. 1743–1759.
- [24] B. PEHERSTORFER AND K. WILLCOX, *Detecting and adapting to parameter changes for reduced models of dynamic data-drive application systems*, Procedia Computer Science, 51 (2015), pp. 2553–2562.
- [25] B. PEHERSTORFER AND K. WILLCOX, *Online adaptive model reduction for nonlinear systems via low-rank updates*, SIAM Journal on Scientific Computing, 37 (2015), pp. 2123–2150.
- [26] S. PRAJNA, *Pod model reduction with stability guarantee*, in 42nd IEEE International Conference on Decision and Control (IEEE Cat. No.03CH37475), vol. 5, 2003, pp. 5254–5258 Vol.5, <https://doi.org/10.1109/CDC.2003.1272472>.
- [27] E. QIAN, B. KRAMER, B. PEHERSTORFER, AND K. WILLCOX, *Lift & learn: Physics-informed machine learning for large-scale nonlinear dynamical systems*, Physica D: Nonlinear Phenomena, 406 (2020), p. 132401.
- [28] C. E. RASMUSSEN AND C. K. I. WILLIAMS, *Gaussian processes for machine learning*, MIT Press, 2005.
- [29] S. SARGSYAN, S. L. BRUNTON, AND J. N. KUTZ, *Nonlinear model reduction for dynamical systems using sparse sensor locations from learned libraries*, Physical Review E, 92 (2015), p. 033304.
- [30] N. T. SON, *A real time procedure for affinely dependent parametric model order reduction using interpolation on grassmann manifolds*, International Journal of Numerical Methods in Engineering, 8 (2013), pp. 818–833.
- [31] D. SORENSEN, *Passivity preserving model reduction via interpolation of spectral zeros*, in 2003 European Control Conference (ECC), 2003, pp. 974–978, <https://doi.org/10.23919/ECC.2003.7085085>.
- [32] F. VETRANO, C. LE GARREC, G. MORTCHELEWICZ, AND R. OHAYON, *Assessment of strategies for interpolating pod based reduced order model and application to aeroelasticity*, Journal of Aeroelasticity and Structural Dynamics, 2 (2011), pp. 85–104.
- [33] Z. YAN, W. LIU, Z. TANG, X. LIU, N. ZHANG, M. LI, AND H. ZHANG, *Review on thermal analysis in laser-based additive manufacturing*, Optics & Laser Technology, 106 (2018), pp. 427–441.
- [34] K. YE AND L. H. LIM, *Schubert varieties and distances between subspaces of different dimensions*, SIAM Journal on Matrix Analysis and Applications, 37 (2016), pp. 1176–1197.
- [35] R. D. ZHANG, S. MAK, AND D. DUNSON, *Gaussian process subspace prediction for model reduction*, SIAM Journal on Scientific Computing, 44 (2022), pp. A1428–A1449.